AVO Analysis—Tutorial and Review

*John P. Castagna**

INTRODUCTION

In conventional utilization of the seismic reflection method, it has traditionally been assumed that seismic signals can be viewed as a band-limited normal incidence reflection coefficient series with appropriate traveltime and amplitude variation due to propagation through an overburden. Ostrander (1982) demonstrated that gas sand reflection coefficients vary in an anomalous fashion with increasing offset and showed how to utilize this anomalous behavior as a direct hydrocarbon indicator on real data. This work popularized the methodology which has come to be known as amplitude variation with offset analysis (AVO). In addition to being a "seismic lithology" tool, AVO provides an improved model of the reflection seismogram which allows us to better estimate both normal incidence reflection coefficients and "background" velocities.

Exploration geophysics is, to a large extent, a science of anomalies. It is probably safe to assume that most hydrocarbons found in the past fifty years have been associated with some kind of geophysical anomaly. Explorationists routinely utilize deviations from expected gravity, seismic traveltime, and seismic amplitude, without recovering uniquely determined absolute density, depth, or reflectivity. Consequently, significant risk is associated with drilling a well, even when all the technology and analysis available have been thrown at the problem. Experience has shown that geophysical anomalies can be used to reduce risk, and consequently, to identify new prospects.

Thus, one would expect the exploration geophysicist, who is concerned primarily with finding hydrocarbons, to have somewhat different expectations from AVO analysis, than say a research physicist, who may be primarily concerned with getting the right answer. Taking the latter approach, if one makes very simplistic assumptions, methods can be developed which work well on synthetic data. However, the more one appreciates the complexities of the real world with real geology, the more it becomes apparent that AVO analysis doesn't work. The only fault with this conclusion is that explorationists are successfully using AVO anomalies to find hydrocarbons throughout the world. The explorationist does not require answers that are correct in absolute terms. The presence of a deviation from some background trend may be sufficient; the magnitude of the deviation in absolute units may not even be required. An appropriate analogy is the spontaneous potential (SP) log. If I am told that an SP log reading is -30 millivolts at some depth, I cannot interpret the rock properties, even with the most sophisticated modeling and inversion schemes. Of course, the SP log is an anomaly log without a meaningful absolute scale. When I see that -30 millivolts is a significant deviation from the background trend produced by surrounding shales, I realize that the SP log is very valuable indeed in the context of my particular problem—that of identifying sands.

I am not advocating a know-nothing approach to AVO analysis. To the contrary, it is extremely important to understand the physics of wave propagation in a real earth to the best of our ability. This is required to correctly process and appropriately interpret the data, with full recognition of potential pitfalls and the expected applicability of the method to the exploration problem at hand. What I am advocating, is a faith in the inherent robustness of geophysical methods when employed to detect and map anomalies, which should also be applied to AVO analysis.

The purpose of this paper is to provide a tutorial introduction to AVO analysis, in order to lay the foundation for, and to place in context, the more advanced papers which constitute this volume.

OFFSET-DEPENDENT REFLECTIVITY

In exploration geophysics, we only rarely deal with simple isolated interfaces. Nevertheless, we must begin our understanding of offset-dependent reflectivity with the partitioning of energy at just such an inter-

*ARCO Oil and Gas Company

face. We must be careful, however, to remember that most reflections we see are a superposition of events from a series of layers, and will have more complex AVO behavior than will be shown here.

Consider two semi-infinite isotropic homogeneous elastic media in contact at a plane interface. Further, consider an incident compressional plane wave impinging upon this interface. The plane-wave assumption is valid at source-to-receiver distances which are much longer than the wavelength of the incident wave and is generally acceptable for precritical reflection data at exploration depths and frequencies. As shown in Figure 1, reflection at an interface involves energy partition from an incident P-wave to (1) a reflected P-wave, (2) a transmitted P-wave, (3) a reflected S-wave, and (4) a transmitted S-wave. The angles for incident, reflected, and transmitted rays synchronous at the boundary are related according to Snell's law,

$$p = \frac{\sin \Theta_1}{V_{P1}} = \frac{\sin \Theta_2}{V_{P2}} = \frac{\sin \Phi_1}{V_{S1}} = \frac{\sin \Phi_2}{V_{S2}} \qquad (1)$$

where,

V_{P1} = P-wave velocity in medium 1,
V_{P2} = P-wave velocity in medium 2,
V_{S1} = S-wave velocity in medium 1,
V_{S2} = S-wave velocity in medium 2,
Θ_1 = incident P-wave angle,
Θ_2 = transmitted P-wave angle,
Φ_1 = reflected S-wave angle,

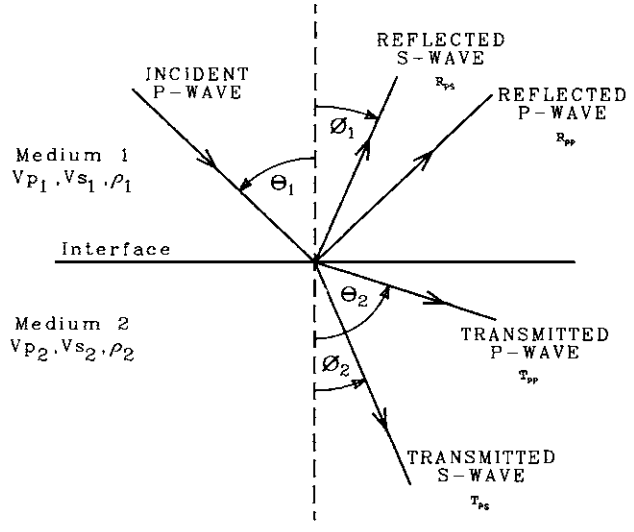

Fig. 1. Reflection and transmission at an interface between two infinite elastic half-spaces for an incident P-wave.

Φ_2 = transmitted S-wave angle,

and p is the ray parameter.

The P-wave reflection coefficient as a function of incidence angle $R_{PP}(\Theta_1)$ is defined as the ratio of the amplitude of the reflected P-wave to that of the incident P-wave. Similarly, the P-wave transmission coefficient $T_{PP}(\Theta_1)$ is the ratio of the amplitude of the transmitted P-wave to that of the incident P-wave. Also, $R_{PS}(\Theta_1)$ is the ratio of the amplitudes of reflected S-wave and incident P-waves, and $T_{PS}(\Theta_1)$ is the ratio of the transmitted S-wave and incident P-wave amplitudes. The following discussion is for particle displacement amplitudes, with polarity assigned according to the horizontal component of displacement.

At normal incidence, there are no converted S-waves and the P-wave reflection coefficient R_P is given by

$$R_P = \frac{I_{P2} - I_{P1}}{I_{P2} + I_{P1}} = \frac{1}{2}\frac{\Delta I_P}{I_{PA}} \approx \frac{1}{2} \ln (I_{P2}/I_{P1}) \qquad (2)$$

where I_P is the continuous P-wave impedance profile,

I_{P2} = impedance of medium 2 = $\rho_2 V_{P2}$,
ρ_2 = density of medium 2,
I_{P1} = impedance of medium 1 = $\rho_1 V_{P1}$,
ρ_1 = density of medium 1,
I_{PA} = average impedance across the interface = $(I_{P2} + I_{P1})/2$, and,
$\Delta I_P = I_{P2} - I_{P1}$.

The logarithmic approximation is acceptable for reflection coefficients smaller than about ± 0.5.

The P-wave transmission coefficient at normal incidence T_P is given by

$$T_P = 1 - R_P \qquad (3)$$

The variation of reflection and transmission coefficients with incident angle (and corresponding increasing offset) is referred to as offset-dependent-reflectivity and is the fundamental basis for amplitude-versus-offset analysis.

Knott (1899) and Zoeppritz (1919) invoked continuity of displacement and stress at the reflecting interface as boundary conditions to solve for the reflection and transmission coefficients as a function of incident angle and the media elastic properties (densities, bulk and shear moduli). By continuity of displacement, it is meant that the interface responds to the incident wave essentially as if the two media were welded together. That is, there is no cavitation (pulling apart) or slippage along the interface. Continuity of normal and

tangential stress is also required to avoid infinite acceleration at the discontinuity.

The resulting Knott and Zoeppritz equations are notoriously complex and subject to troublesome sign, convention, or typographical errors (Hales and Roberts, 1974). Their complexity is such that they yield little physical insight, and the use of digital computers was required before they could be used routinely for exploration applications. Young and Braile (1976) modified expressions from Cerveny and Ravindra (1971) and provided a simple computer subroutine for coefficient calculation. Aki and Richards (1980) and Waters (1981; with obligatory sign error) gave the equations in easily solved matrix form

$$\mathbf{Q} = \mathbf{P}^{-1}\mathbf{R} \tag{4}$$

where **Q**, **P**, and **R** are given in Appendix A.

The coefficients R_{PP}, R_{PS}, T_{PP}, and T_{PS}, at any given incident angle Θ_1 are completely determined by the density and the P-wave and S-wave velocities of each medium. These parameters are, in turn, dependent on medium physical properties such as lithology, porosity, and pore fluid content.

Figure 2 (after Richards, 1961) illustrates the reflection coefficient variation for a variety of impedance ratios with a constant V_P/V_S of 2 in each layer (see Table 1). Keep in mind that Figure 2 shows the entire range of possible incidence angles, whereas common exploration incidence angles are about 30 degrees or less. Some observations follow:

(1) Reflected P-wave amplitude local maxima may occur at normal incidence, the first critical angle, and possibly near the S-wave critical angle. Total internal reflection always occurs at grazing incidence (90 degrees incident angle).

(2) The change of the reflection coefficient with respect to angle of incidence is small at low angles.

(3) The first critical angle Θ_{C1} is given by

$$\sin \Theta_{C1} = \frac{V_{P1}}{V_{P2}}. \tag{5}$$

Readers familiar with the principle of total internal reflection in optics may recall that beyond the critical angle all energy is reflected. This is also true for an interface between two fluid layers. However, for elastic layers, reflected P-wave energy decreases after the first critical angle due to increased conversion to reflected and transmitted S-waves. Consequently, there can be a second critical angle Θ_{C2} given by

$$\sin \Theta_{C2} = \frac{V_{P1}}{V_{S2}}. \tag{6}$$

Beyond this critical angle there are no transmitted S-waves. Note that when V_{P1} is greater than V_{S2} there is no second critical angle, and converted S-waves will be transmitted at all angles below 90 degrees. Similarly, when V_{P1} is greater than V_{P2}, there is no first critical angle, and P-waves can always be transmitted.

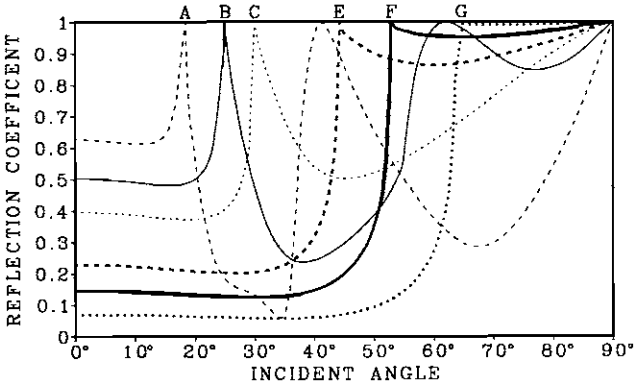

Fig. 2. P-wave reflection coefficient versus incident angle for six models given in Table 1 (after Richards, 1961).

Table 1. Parameters of first layer for six Zoeppritz models from Richards (1961) for Paleozoic limestone structures in Western Canada. These models correspond to reflection coefficient curves given in Figure 2 when the second layer has the parameters: V_P = 20 000 ft/s (6096 m/s), V_S = 10 000 ft/s (3048 m/s), and ρ is 2.65 gm/cc. Note that V_P/V_S = 2 for all layers.

Overburden Model	V_P (ft/s)	V_P (m/s)	V_S (ft/s)	V_S (m/s)	ρ (gm/cc)
A	6000	1829	3000	914	2.02
B	8270	2521	4135	1260	2.12
C	10000	3048	5000	1524	2.20
E	14000	4267	7000	2133	2.38
F	16000	4877	8000	2438	2.47
G	18000	5486	9000	2743	2.56

(4) At near normal incidence, R_{PP} initially decreases very slightly with increasing angle. Deviations from this general behavior can result from changes in V_P/V_S across the interface, and form the basis for seismic lithology analysis.

Some additional features of the Zoeppritz equations are:

(1) S-wave conversions, both reflected and transmitted, are generally strongest between the first critical angle and grazing incidence. S-wave conversions can be very strong at offsets commonly encountered in seismic prospecting.

(2) The reflection coefficient becomes complex beyond the critical angle, and a corresponding phase shift is introduced.

(3) The reflection and transmission coefficients are frequency independent.

(4) The reflection coefficient for a downgoing P-wave incident in medium 1 is generally not equal and opposite to that of an upgoing P-wave incident on the same interface in medium 2. Thus, the reflection coefficient behavior is asymmetrical.

Some exceptions must be considered for spherical waves which exhibit frequency-dependent reflection coefficients and for which the reflection coefficient maximum occurs beyond the critical angle. For most exploration applications, however, the plane-wave assumption is considered adequate.

Muskat and Meres (1940), without the benefit of a computer, calculated reflection coefficient versus angle of incidence for a large number of cases. However, partially due to the lack of information about V_P/V_S ratios in sedimentary rocks available at the time, and perhaps more importantly, due to the very laborious computations required, a constant V_P/V_S ratio of $\sqrt{3}$ (a classical Poisson solid) was assumed for each medium. This assumption colored the exploration community's thinking for many years. By assuming constant V_P/V_S, one is led to the conclusion that, for exploration geometries, amplitude decreases with increasing angle of incidence, and the overall effect is rather small. In fact, this conclusion provided theoretical justification for such procedures as stacking, convolutional modeling, bright spot analysis, and one dimensional (1-D) seismic inversion. The assumption that stacked reflection amplitudes mimic normal incidence reflection coefficients has been very effectively exploited by seismic interpreters. However, the potential of AVO analysis was generally overlooked. Application of AVO was limited to a few special cases (Anstey, 1977): (1) A weak target reflector can be intentionally illuminated at the critical angle to obtain a stronger signal. (2) As previously noted, if V_{P1} is greater than V_{P2}, no critical angle amplitude maximum will be observed. Thus, the polarity of the reflection may be identified if long offsets are available. (3) In some cases, salt reflections can be identified by a characteristic increase of amplitude with offset caused by an increase in velocity accompanied by a decrease in density across the interface.

Now let us turn our attention to the precritical angle of incidence range which is most important for exploration applications. Koefoed (1955) first pointed out the practical possibilities of using AVO analysis as an indicator of V_P/V_S variations. Figure 3 shows some of his reflection coefficient versus angle curves. Note that the calculations were restricted only to angles of incidence likely to be encountered in seismic exploration, and that the Poisson's ratio was allowed to vary across the interface (see Table 2 for model parameters). Poisson's ratio σ is related to V_P/V_S by

$$\sigma = \frac{\frac{1}{2}\left(\frac{V_P}{V_S}\right)^2 - 1}{\left(\frac{V_P}{V_S}\right)^2 - 1}, \tag{7a}$$

and

$$\frac{V_S}{V_P} = \sqrt{\frac{\frac{1}{2} - \sigma}{1 - \sigma}}. \tag{7b}$$

Figure 3 forms the empirical basis for some very general conclusions (Koefoed's rules) concerning the information content of reflection coefficients which will be discussed in a later section. Some additional observations are: (1) Figure 3a, 3b, and 3c illustrate the basic principle exploited when AVO is used for hydrocarbon detection; as σ_2 decreases (as would occur when gas replaces brine), the reflection coefficient becomes more negative with increasing offset. Contrast this to the often abused rule of thumb that "gas causes amplitude to increase with offset" which is only correct for near zero or negative R_P (keep in mind that increased "amplitude" results from increasing the magnitude of the reflection coefficient in a positive or negative direction). (2) For $\Delta\sigma = 0$ (Figures 3d and 3f), lowering the average Poisson's ratio, $(\sigma_1 + \sigma_2)/2$, also causes the reflection coefficient to become more negative with increasing offset. (3) Comparison of Figures 3b and 3e shows that the effect of lowering σ_2 occurs for all V_{P2}/V_{P1} ratios. (4) If V_{P2}/V_{P1} is

varied while density and Poisson's ratio remain constant, the magnitude of the AVO effect is essentially unchanged (the AVO curves are shifted by the normal incidence reflection coefficient R_P).

Koefoed (1955) suggested what is today a somewhat overlooked application, that of using characteristic AVO responses to help correlate across faults. More prophetically he stated:

"... in a more remote future it may become possible to draw conclusions concerning the lithological nature of rock strata from the shapes of the reflection coefficient curves of the interfaces by which they were bounded."

APPROXIMATIONS TO THE KNOTT AND ZOEPPRITZ EQUATIONS

The unwieldy nature of the Knott-Zoeppritz equations defies physical insight and makes visualizing how the variation of a particular parameter will effect the reflection coefficient curve very difficult. Approximations are extremely useful for practical applications as they more readily reveal the information content contained in the amplitude behavior, do not require a computer to evaluate, and provide the basis for certain AVO processing techniques.

Bortfeld (1961) linearized the Zoeppritz equations by assuming small changes in layer properties and obtained

$$R_{PP}(\Theta_1) \approx \frac{1}{2} \ln \left[\frac{V_{P2}\rho_2 \cos \Theta_1}{V_{P1}\rho_1 \cos \Theta_2} \right] + \left(\frac{\sin \Theta_1}{V_{P1}} \right)^2 (V_{S1}^2 - V_{S2}^2) \times \left[2 + \frac{\ln \left(\frac{\rho_2}{\rho_1} \right)}{\ln \left(\frac{V_{S2}}{V_{S1}} \right)} \right]. \quad (8)$$

This approach was also followed in Richards and Frasier (1976) and Aki and Richards (1980) who derived a form simply parameterized in terms of the changes in density, P-wave velocity, and S-wave velocity across the interface:

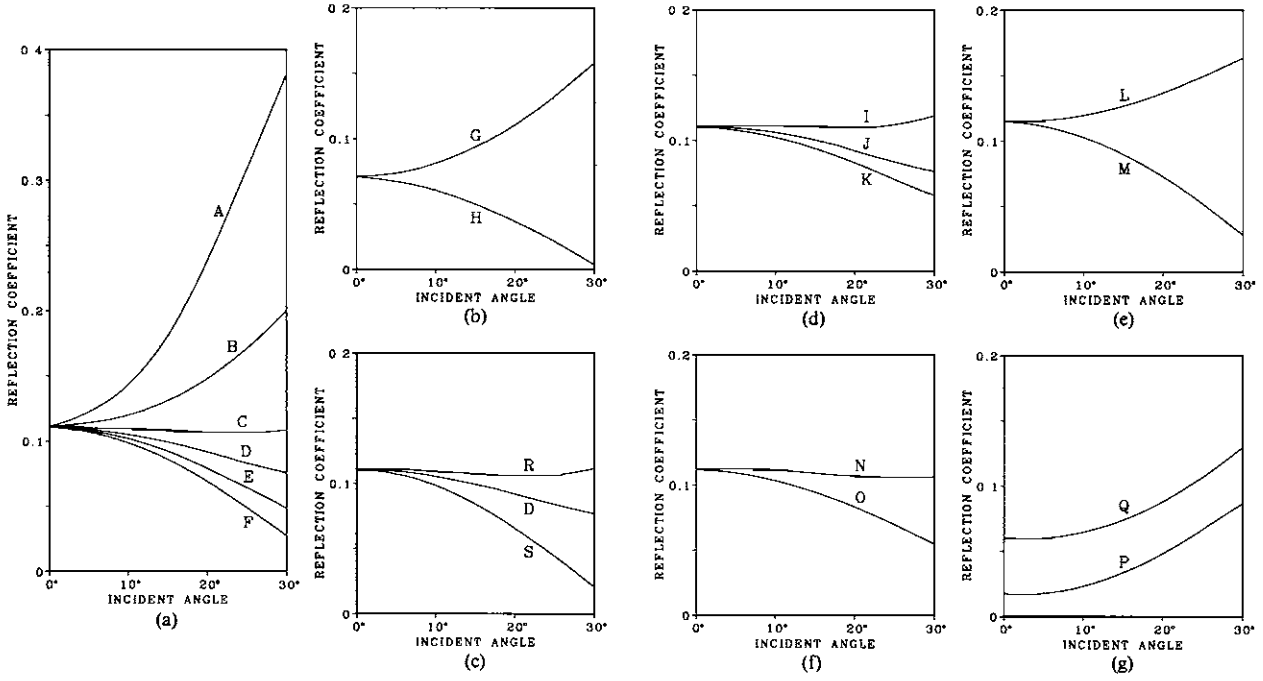

Fig. 3. P-wave reflection coefficient versus incident angle for model parameters given in Table 2 (from Koefoed, 1955). (a) and (b) show varying Poisson's ratio in the second medium, (c) and (e) show varying Poisson's ratio in the first medium, (d) shows varying values of Poisson's ratio which is equal in both half-spaces, and (f) shows varying values of the P-wave velocity contrast.

$$R_{PP}(\Theta) \approx \frac{1}{2}(1 - 4p^2V_{Sa}^2)\left(\frac{\Delta\rho}{\rho_a}\right) + \frac{1}{2\cos^2(\Theta)} \times \frac{\Delta V_P}{V_{Pa}} - 4p^2V_{Sa}^2\frac{\Delta V_S}{V_{Sa}} \quad (9)$$

where

$$\begin{aligned} \Delta_\rho &= \rho_2 - \rho_1, \\ \Delta V_P &= V_{P2} - V_{P1}, \\ \Delta V_S &= V_{S2} - V_{S1}, \\ \rho_a &= (\rho_2 + \rho_1)/2, \\ V_{Pa} &= (V_{P2} + V_{P1})/2, \\ V_{Sa} &= (V_{S2} + V_{S1})/2, \\ \Theta &= (\Theta_1 + \Theta_2)/2 \end{aligned}$$

and p is the ray parameter as defined by equation (1). Because interchanging the medium properties simply changes the sign of $\Delta\rho$, ΔV_P, and ΔV_S, we see that equation (9) is fundamentally different from the Zoeppritz equations in that the reflection coefficient is symmetrical. According to Backus (1992; personal communication) for reflections from layers rather than from isolated interfaces, superposition of the P-wave and the locally converted S-wave may roughly cancel the asymmetry predicted by the Zoeppritz equations for primaries only. Thus, for some uses, the Aki and Richards approximation is more appropriate than the exact Zoeppritz equations. As a further approximation, Θ_1 is usually used rather than Θ.

For the special case of fluid layers, the reflection coefficient is given exactly by

$$R_{PP}(\Theta_1) = \frac{V_{P2}\rho_2\cos\Theta_1 - V_{P1}\rho_1\cos\Theta_2}{V_{P2}\rho_2\cos\Theta_1 + V_{P1}\rho_1\cos\Theta_2}. \quad (10)$$

Equation 10 is referred to as the "acoustic" reflection coefficient, $R_f(\Theta_1)$, rather than "fluid factor" as originally used by Hilterman and later used in Smith and Gidlow (1987) to mean something entirely different (see following discussion). Hilterman's course notes pointed out the physical insight to be gained by separating the Bortfeld approximation into "fluid" and "shear" terms. He recognized that the first term of the Bortfeld equation is about equal to equation (10) and modified Bortfeld's equation such that

$$R_{PP}(\Theta_1) = R_f(\Theta_1) + R_{sf}(\Theta_1) \quad (11)$$

where, $R_{sf}(\Theta_1)$, is the "shear factor" given by

$$R_{sf}(\Theta_1) = \left(\frac{\sin\Theta_1}{V_{P1}}\right)^2 (V_{S1} + V_{S2})\left[3(V_{S1} - V_{S2}) + 2\frac{V_{S2}\rho_1 - V_{S1}\rho_2}{\rho_2 + \rho_1}\right]. \quad (12)$$

Table 2. Parameters for Zoeppritz models from Figure 3 (Koefoed, 1955).

Model	ρ_2/ρ_1	V_{P2}/V_{P1}	σ_1	V_{P1}/V_{S1}	σ_2	V_{P2}/V_{S2}
A	1.0	1.25	.25	1.73	.50	∞
B	1.0	1.25	.25	1.73	.40	2.45
C	1.0	1.25	.25	1.73	.30	1.87
D	1.0	1.25	.25	1.73	.25	1.73
E	1.0	1.25	.25	1.73	.20	1.63
F	1.0	1.25	.25	1.73	.15	1.56
G	1.0	1.15	.25	1.73	.40	2.45
H	1.0	1.15	.25	1.73	.15	1.56
I	1.0	1.25	.40	2.45	.40	2.45
J	1.0	1.25	.25	1.73	.25	1.73
K	1.0	1.25	.15	1.56	.15	1.56
L	1.0	.80	.40	2.45	.25	1.73
M	1.0	.80	.15	1.56	.25	1.73
N	1.0	.80	.40	2.45	.40	2.45
O	1.0	.80	.15	1.56	.15	1.56
Q	.9	1.25	.25	1.73	.36	2.14
P	.9	1.15	.25	1.73	.36	2.14
R	1.0	1.25	.15	1.56	,25	1.73
S	1.0	1.25	.40	2.45	.25	1.73

For larger contrasts between layer properties, R_{sf} can be multiplied by $[1 - R_f(\Theta_1)^2]$ to better approximate the full Zoeppritz equations (Banik, personal communication).

Separation of the Bortfeld equations into "acoustic or fluid" and "shear" terms can also be achieved by assuming constant density (Hilterman, unpublished course notes, 1983) with

$$R_{PP}(\Theta_1) \approx \frac{V_{P2}\cos\Theta_1 - V_{P1}\cos\Theta_2}{V_{P2}\cos\Theta_1 + V_{P1}\cos\Theta_2} + 2\left(\frac{\sin\Theta_1}{V_{P1}}\right)^2 (V_{S1}^2 - V_{S2}^2) \quad (13)$$

Figure 4, after Hilterman (unpublished course notes, 1983), illustrates the effect of the shear factor. Note that varying the shear factor may cause $R_{PP}(\Theta_1)$ to increase or decrease with increasing offset.

Shuey (1985) presented another form of the Aki and Richards (1980) approximation

$$R_{PP}(\Theta_1) \approx R_P + \left(A_0 R_P + \frac{\Delta\sigma}{(1-\sigma)^2}\right)\sin^2\Theta_1 + \frac{1}{2}\frac{\Delta V_P}{V_{Pa}}(\tan^2\Theta_1 - \sin^2\Theta_1) \quad (14)$$

where, R_P, is the normal incidence reflection coefficient, A_0 is given by

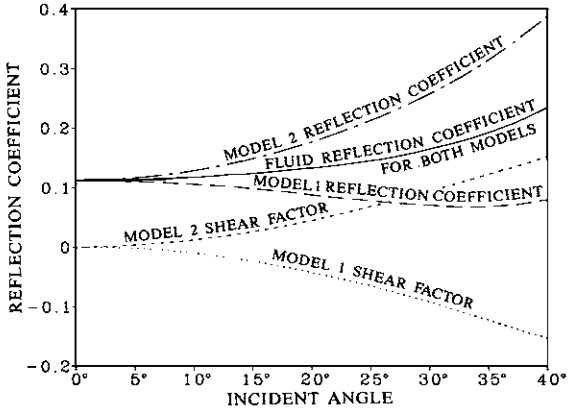

Fig. 4. The effect of the shear term, R_{sf}, on the P-wave reflection coefficient for two models. Model 1 has V_{P1} = 10 000 ft/s (3048 m/s), V_{P2} = 12 500 ft/s (3810 m/s), Poisson's ratio equals .25 for both media and density is constant. Model 2 is the same except Poisson's ratio is .1 for medium 1 and .4 for medium 2 (after Hilterman, unpublished course notes, 1983).

$$A_0 = B_0 - 2(1 + B_0)\left(\frac{1-2\sigma}{1-\sigma}\right) \quad (15)$$

and

$$B_0 = \frac{\dfrac{\Delta V_P}{V_{Pa}}}{\dfrac{\Delta V_P}{\Delta V_{Pa}} + \dfrac{\Delta\rho}{\Delta\rho_a}}. \quad (16)$$

The advantage of this form is that each term simply describes a different angular range of the offset curve. The first term is the normal incidence reflection coefficient, the second term predominates at intermediate angles, and the third term is dominant as the critical angle is approached. Thus, for restricted angles of incidence, we have an equation linear in $\sin^2\Theta_1$.

$$R_{PP}(\Theta_1) \approx R_P + B\sin^2\Theta_1. \quad (17)$$

One often sees "A" used to represent the normal incidence reflection coefficient R_P. B is called the "AVO gradient" and is given by

$$B = A_0 R_P + \frac{\Delta\sigma}{(1-\sigma)^2}. \quad (18)$$

Wiggins et al. (1983) showed that if V_P/V_S is about 2, for small angles then

$$B = R_P - 2R_S. \quad (19)$$

This approximation greatly simplifies AVO interpretations.

The coefficients of the Wiggins and Shuey approximations are easily obtained by linear regression and form the basis of various "weighted stacking" procedures (see for example Smith and Gidlow, 1987).

Hilterman (1989) derived another convenient approximation:

$$R_{PP}(\Theta_1) \approx R_P\cos^2\Theta_1 + 2.25\Delta\sigma\sin^2\Theta_1. \quad (20)$$

Thus, at small angles R_P dominates the reflection coefficient, whereas $\Delta\sigma$ dominates at larger angles. Thus, one can think of a near offset stack as imaging P-wave impedance contrasts, while the far offset stack images Poisson's ratio contrasts.

INFORMATION CONTENT

Koefoed (1955; see Figure 3) empirically established five rules which were later verified in Shuey (1985) for moderate angles of incidence:

(1) "When the underlying medium has the greater

longitudinal (P-wave) velocity and other relevant properties of the two strata are equal to each other, an increase of Poisson's ratio for the underlying medium causes an increase of the reflection coefficient at the larger angles of incidence." Shuey (1985) points out that the qualifications concerning the medium properties are not necessary for this and the next rule.

(2) "When, in the above case, Poisson's ratio for the incident medium is increased, the reflection coefficient at the larger angles of incidence is thereby decreased."

(3) "When, in the above case, Poisson's ratios for both media are increased and kept equal to each other, the reflection coefficient at the larger angles of incidence is thereby decreased." This is strictly true only when Shuey's parameter B is greater than -1.

(4) "The effect mentioned in (1) becomes more pronounced as the velocity contrast becomes smaller."

(5) "Interchange of the incident and the underlying medium affects the shape of the curves only slightly, at least up to the values of the angle of incidence of about 30 degrees." In other words, the reflection coefficient is nearly, but not quite, symmetrical at moderate angles.

For constant P-wave velocity and density, rules (1) and (3) imply that various combinations of Poisson's ratio can result in the same variation of the reflection coefficient with offset. This means that the inversion of the Zoeppritz equations for Poisson's ratio is fundamentally nonunique. Rosa (1976) demonstrated this analytically by differentiating the Zoeppritz equations with respect to the various model parameters. Figure 5 implies that many combinations of σ_1 and σ_2 can have the same reflection coefficient.

This was rediscovered and reported in Morley (1984) and de Haas and Berkhout (1988) among others. Figure 6, from the latter paper, shows the error in predicted reflection coefficient of a particular model as σ_1 and σ_2 are varied. Morley (1984) goes on to state that little information over post-stack inversion is obtained if amplitudes are only measured out to half of the critical angle. This has led some workers to suggest that multicomponent data are required for unambiguous inversion (see following discussion). Of course, if inversion for absolute Poisson's ratio is not required, the outlook for successful utilization of conventional AVO data is brighter.

Aki and Richards (1980), Wiggins (1983), and Shuey (1985) show that the additional information obtainable by AVO analysis is $\Delta\sigma$ (or equivalently R_S). Fortunately, this may be sufficient for many applications.

As the incident angle aperture increases, the third term in Shuey's approximation becomes significant

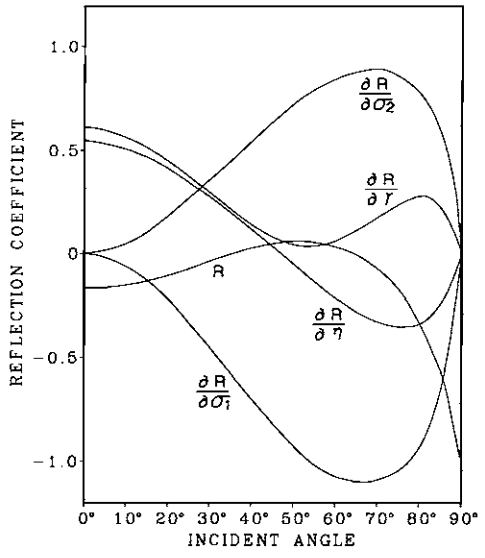

Fig. 5. The reflection coefficient for P-waves as a function of incidence angle and its partial derivatives with respect to the elastic parameters (from Rosa, 1976). $\gamma = V_{P2}/V_{P1} \cdot \zeta = \rho_2/\rho_1$.

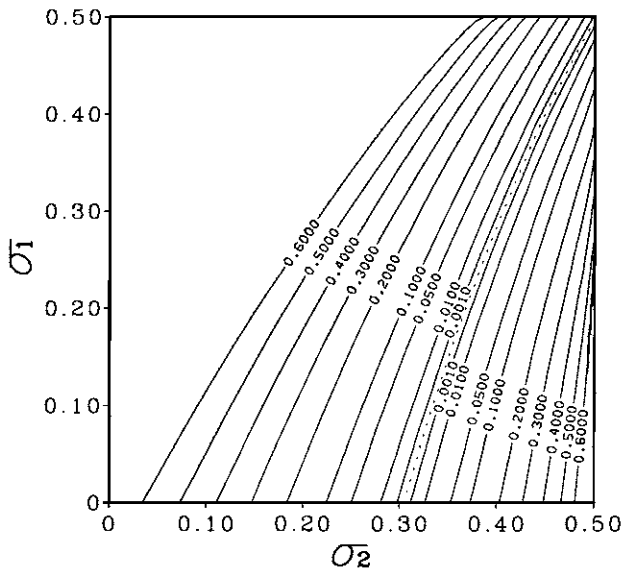

Fig. 6. Error in predicted reflection coefficient as Poisson's ratio in each medium is varied from the "true" Poisson's ratio of .1014 in medium 1 and .3333 in medium 2. The P-wave velocity ratio between the two media is .8, and the density ratio is .9 (from de Haas and Berkhout; 1988).

(e.g., Dey-Sarkar and James, 1986; Balogh and Snyder, 1986) and provides new information (P-wave velocity contrast from which density contrast can be unraveled). Even with an incident angle of 45 degrees, recovery of the third term is less robust than second term recovery. Nevertheless, Parson (1986) showed promising results for three-parameter gradient separation. The three parameter fit to $R_{PP}(\Theta_1)$ is important in direct detection since it can potentially provide a distinction between bright spots caused by low or high gas saturations.

PETROPHYSICAL BASIS

Gassmann's (1951) equations provide the fundamental basis for direct hydrocarbon indication. These equations predict a large drop in P-wave velocity and a small increase in S-wave velocity when even a small amount of gas is introduced into the pore space of a compressible brine-saturated sand. This drop (along with the corresponding density change) changes the P-wave reflection coefficient (resulting in "bright" or "dim" spots) and causes a drop in V_P/V_S (which causes AVO anomalies).

Ultrasonic laboratory measurements (such as Gregory, 1976; Domenico, 1976) do not quantitatively agree with Gassmann predictions. However, low-frequency laboratory measurements (Murphy, 1982) show excellent agreement with Gassmann's equations (see Figure 7). For seismic frequencies, we assume the Gassmann's equations are generally valid for sandstones. Gassmann's equations are strictly valid only when the following assumptions are applicable: (1) The porous rock framework (skeleton) is macroscopically isotropic and homogeneous. (2) The skeleton, grains, fluids, and saturated rock obey Hooke's law (stress is proportional to strain), and (3) The pore space is interconnected, fluid pressure is uniform, no fluid enters or leaves any volume of the system, and no cavitation occurs. It would seem that the shalier the rock, the more likely it is these assumptions will be violated.

Oil and water are often assumed to have similar acoustic properties, and to be indistinguishable with seismic methods. However, recent work (Rafipour, 1987; Wang et al., 1990) suggests that compressible oils with high gas-oil-ratio (GOR) may be detectable. Figure 8 shows predicted sonic log transit-times in an offshore Gulf of Mexico oil sand for various pore fluids. It is important to distinguish "live" oil from "dead" oil properties. Under in-situ pressure-temperature conditions, oils contain some amount of dissolved gas and are said to be "live". When the oil is

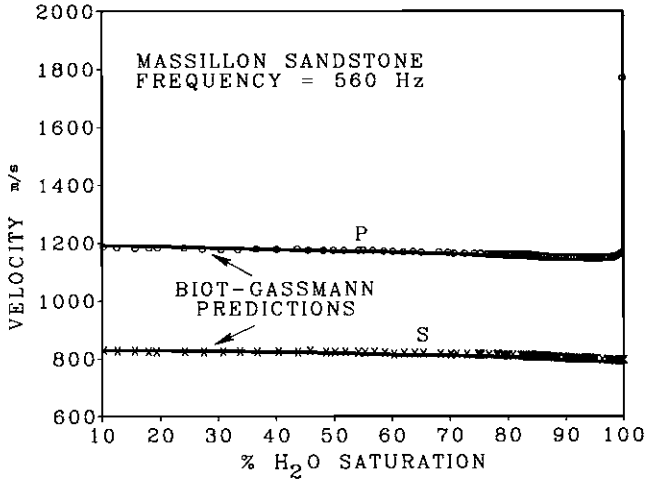

Fig. 7. Bar resonance data of Murphy (1982) for Massillon sandstone. The data are in agreement with Gassmann's equations (solid lines).

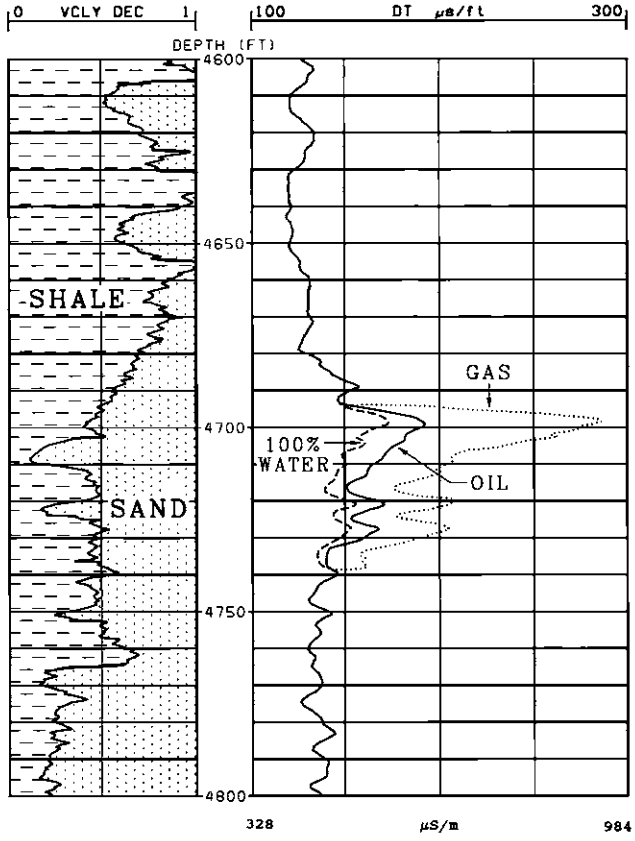

Fig. 8. Sonic log through an oil sand and calculated sonic logs for various Gassmann fluid substitutions.

produced, gas comes out of solution as the oil equilibrates to surface conditions leaving the oil "dead". The amount of exsolved gas is used to determine the GOR. It is important to note, as seen in Figure 8, that "live" oil-saturated sandstone can be significantly slower than water-saturated rock.

Angerer and Richgels (1990) describe various factors affecting P-wave and S-wave velocity: mineralogy, porosity, pore fluids, depth of burial, pressure, and temperature. Pore shape distribution and degree of lithification are also important factors. To first order, porosity, depth of burial, pressure, and lithification generally affect V_P and V_S in the same way. Thus, excepting unusual pore shapes, a given lithology will have a well defined V_P-V_S relationship. Given V_P and lithology, Greenberg and Castagna (1992) showed that S-wave velocity prediction can be quite robust, however, the prediction error (about 5 percent) may be inadequate when viewed in terms of reflection coefficients.

Locally calibrated V_P-V_S and V_P-ρ trends may provide essential a priori information for AVO analysis and may transform a nonunique seismic inversion problem into a well-constrained hydrocarbon detection scheme. Two parameters extractable by AVO analysis, R_P and R_S, can be crossplotted to identify gas sands in a clastic stratigraphic section. We use V_P-V_S and V_P-ρ trend curves (Castagna et al., 1993 this volume, pages 135–171.) for shale, brine sand, and gas sand. We also use the following empirical equation for gas sands:

$$\rho^{gs} = .199V_P^{gs} + 1.53 \qquad (21)$$

where ρ^{gs} is gas-sand density and V_P^{gs} is gas-sand velocity in km/s. The reader is cautioned that local calibration of trends (particularly V_P-ρ) is strongly recommended.

Figure 9 shows shale over brine sand and shale over gas sand reflection coefficients for a range of shale V_P ranging from 1.5 to 5.5 km/s. (A similar plot for shale over shale reflection coefficients is very similar to the shale over brine sand plot). Some very significant observations can be made:

(1) Large negative P-wave reflection coefficients (R_P less than $-.1$): Gas sand and brine sand reflections are unambiguously separated. The more negative the P-wave reflection coefficient or the lower the shale velocity, the greater the separation between gas and brine sands.

(2) Near-zero P-wave reflection coefficients (R_P between $-.1$ and .1): Gas sand and brine sand reflection coefficients are unambiguously separated only for low shale velocities (less than about 3.5 km/s) and only if shale velocity is approximately known.

(3) Large positive P-wave reflection coefficients (R_P greater than .1): Gas sand and brine sand reflection coefficients are unambiguously separated only for the lowest shale velocities (less than about 2.5 km/s) and only if the shale velocity is approximately known. The separation decreases with increasing R_P.

Similarly, comparison of Figure 9 with Figure 10 shows that the gas-sand over brine-sand (or shale) reflection can be distinguished from a shale over brine-sand reflection providing the expected gas-sand

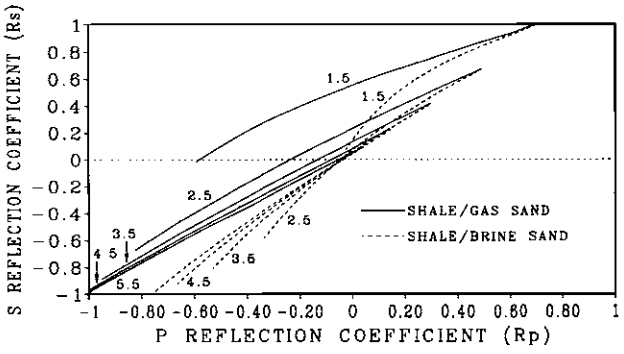

Fig. 9a. Reflection coefficients for shale over gas sand interface (solid) and shale over brine sand interface (dashed) for shale velocities ranging from 1.5 to 5.5 km/s.

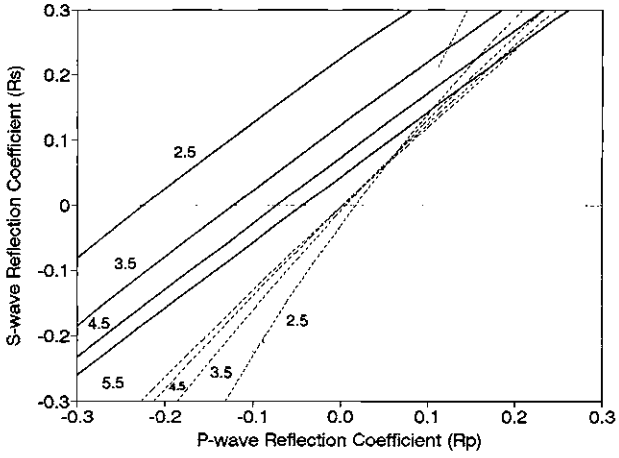

Fig. 9b. Expanded view of Figure 9a to emphasize the reflection coefficient range which is most appropriate for exploration applications.

velocity is less than about 4.5 km/s. Furthermore, if we assume equal porosity above and below the gas-water contact, R_S is about zero.

For completeness, note that gas sand over gas sand reflections are characterized by $R_P = R_S$ as V_P/V_S is approximately constant.

These R_P-R_S crossplots cover a very broad range of velocities. In practice, the range of expected velocities is much more limited. In general, velocity-depth functions for sands and shales can be constructed from well logs, or velocity analyses and petrophysical concepts. For example, a particular offshore Louisiana region has the following average properties above geopressure:

$$V_P^{sh} = .394\ Z + 1.73 \tag{22a}$$

and

$$V_P^{ss} = 1.12\ V_P^{sh} - .24 \tag{22b}$$

where

V_P^{sh} = shale P-wave velocity in km/s,
V_P^{ss} = sandstone P-wave velocity in km/s, and
Z = depth (km).

Combining equations (22a) and (22b) with V_P-V_S and V_P-ρ trend curves, yields R_P/R_S as a function of depth for shale over brine sand and shale over gas sand reflections. As shown in Figure 11, R_P/R_S is an excellent gas indicator at shallow depths but becomes less discriminating as depth increases. By carrying error bars with the R_P/R_S versus depth trends, and knowing the error bars for the AVO analysis, one can compute a confidence in the hydrocarbon indication. As R_P/R_S becomes unstable at small R_S, the difference R_P minus R_S may be a preferable indicator in some instances. A similar approach can be used to investigate the effects of coal or other lithologies.

An important word of caution: errors in the extraction of R_P and R_S tend to be biased (by anisotropy for example; see the following section) and the results may not conform to our petrophysical expectations. When this is the case, one should be willing to move the non-pay "baseline", as is commonly done in well log analysis, to empirically correct these biases (see also Smith and Gidlow, 1987; Spratt et al., 1993 this volume, pages 37–56.). With this empirical approach, the role of petrophysics differs from the forward modeling and inversion approaches. Petrophysical analysis provides: (1) The expected systematics of variation (for example; gas sands should plot to the upper left on Figure 9). (2) The expected magnitude of the anomaly and the petrophysical S/N. (3) The expectation of petrophysical uniqueness (or lack thereof) of the indicator, and (4) The basis for exploration where sufficient empirical data are not available.

COMPLICATING FACTORS, PROBLEMS, AND PITFALLS

All too often, the tremendous potential of AVO analysis as a prospecting tool has not been realized partially because of the wide variety of complications, problems, and pitfalls involved in isolating and interpreting the offset-dependent-reflectivity (ODR). Table 3 shows the myriad of factors affecting seismic amplitudes. For most AVO analysis techniques, all factors other than reflection coefficient variation with offset must be considered undesired noise (which should be attacked by processing or properly accounted for) or

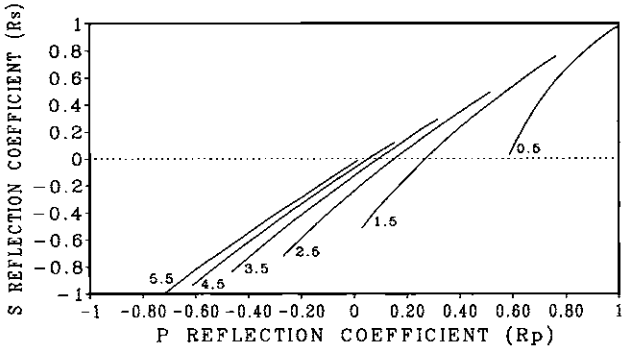

Fig. 10. Reflection coefficients for gas sand over shale interface for gas sand velocities ranging from 1.5 to 5.5 km/s. R_P/R_S is always less than unity. Comparison to Figure 9 shows for gas sand velocities less than 4.5 km/s that there is no overlap with shale over brine sand (or brine sand over shale) reflection coefficients.

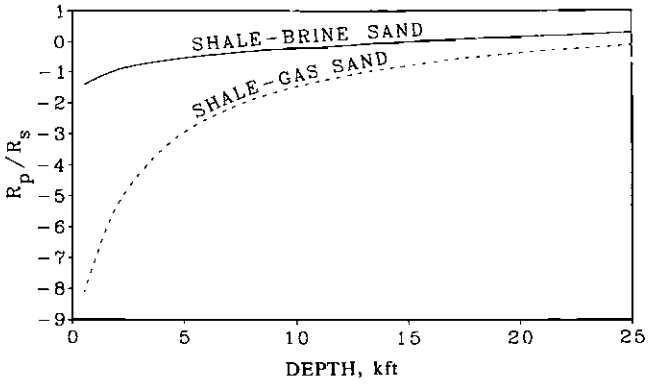

Fig. 11. AVO sensitivity for a particular Louisiana area. R_P/R_S versus depth for shale over brine sand and shale over gas sand interfaces.

must be appropriately comprehended as signal by the processing/analysis techniques. We must always be aware of the angle-dependent total system response/ wavelet variation when attempting to isolate ODR.

Composite Reflections

According to Sherwood et al (1983): "The simple interface reflection coefficient is only a starting point toward understanding offset-dependent-reflectivity. More often we deal with reflections from layers, transition zones, or complex layered sequences." Modeling and inversion are required to resolve the effects of superposition of reflections from more than one interface.

The classical bed tuning phenomenon (Widess, 1973) becomes more complex when considered as a function of offset. Ostrander (1984), Hindlet and McDonald (1986), Ball (1988), and Swan (1988) among others considered this phenomenon. As shown in Ostrander (1984), the apparent change in time thickness of a layer is approximately obtained by differentiating the normal moveout equation. Also

$$\frac{\Delta t_\Theta}{\Delta t_0} \approx \cos \Theta \qquad (23)$$

where t_0 is the normal incidence arrival time and t_θ is the arrival time for angle θ in the layer. Figure 12 from Ostrander (1983 unpublished course notes) shows that tuning can cause amplitude to increase or decrease with offset depending on the normal incidence time thickness-frequency product. With increasing offset, the time thickness decreases and the amplitude varies according to Figure 12.

Table 3. Factors affecting seismic amplitudes.

A. Desired information (signal)
1. reflection coefficients versus angle of incidence
B. Potential information (considered noise for some methods; signal for others)
1. composite reflections from multiple interfaces
2. tuning caused by NMO convergence
3. mode conversions
C. Factors without offset dependence (noise)
1. random noise
2. instrumentation
3. source/receiver coupling
D. Factors with offset dependence (noise)
1. source/receiver directivity including ghosting and array response
2. emergence angles
3. coherent noise, multiples
4. spherical spreading
5. processing distortions, NMO errors and stretch
6. inelastic attenuation and anisotropy
7. transmission coefficients and scattering above target
8. structural complexity

Near Surface Considerations

There are a variety of near surface effects which perturb seismic amplitudes. Source strength and receiver coupling variations, particularly when related to slowly varying near-surface impedance or surface conditions, can modify AVO. Surface-consistent processing can be used to combat this. Other obvious emergent angle dependent effects include, source radiation pattern, geophone response, and array response. These effects are well known and readily corrected. Energy partitioning due to free surface mode conversions can also be corrected (Cerveny and Ravindra, 1971). In the marine case, angle dependent ghosting is considered a second-order problem. Near-surface transmission effects may also be important (see following discussion).

General Data Quality Issues

Seismic data quality is the most fundamental requirement for successful AVO analysis. Sufficient signal-to-noise (S/N), bandwidth, aperture (offset),

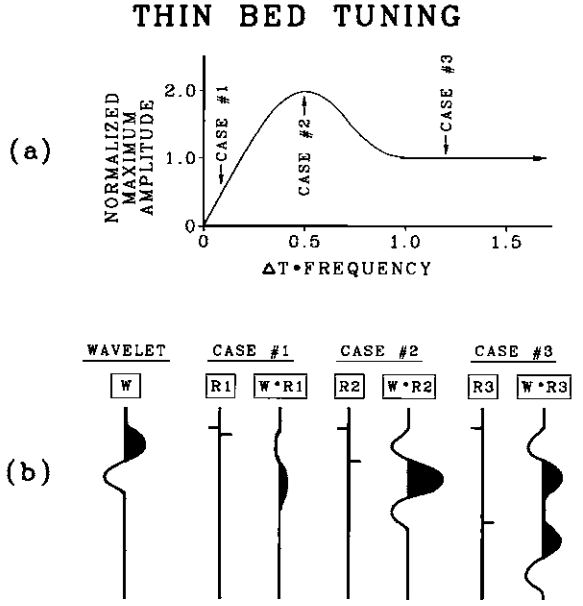

Fig. 12. (a) Normalized maximum amplitude versus frequency-time thickness product showing effect of thin bed tuning. Cases 1, 2, and 3 are indicated. (b) Convolution of wavelet with three reflectivity series R1, R2, and R3 which are below, at, and above tuning, respectively (from Ostrander, unpublished course notes, 1983).

and fold are all basic requirements. Channels, if not amplitude calibrated, must at least be consistent throughout the survey. Channel balancing may be problematical. As pointed out in Frasier (1988), individual traces have lower S/N than stacked traces, so channel balancing attempts may only balance the noise.

Source-generated coherent noise in the form of multiples, converted waves, diffractions, etc. is particularly troublesome. As shown in Pan et al. (1990) incoherent noise is less of a problem.

To suppress coherent noise *f-k* filtering is often applied. However, coherent noise, such as multiples, with varying spatial frequency (moveout) across a gather, may be unevenly attenuated, thereby biasing the AVO estimate. Multiples can also be attacked by ray parameter filtering or by predictive deconvolution in various domains. Multiples with small residual moveout (1/2 to 1 cycle) create a false amplitude variation with offset and are extremely difficult to remove. This is probably the single most important data quality issue for marine AVO.

A great promise of full-waveform inversion is that certain source-generated noise may become signal.

Curvature and Structural Complexity

By analogy with optics, we expect curved interfaces to act as lenses and curved mirrors, concentrating or dispersing seismic energy. Hilterman (1975) defined the curvature effect (CE) for a reflecting interface as the ratio of the reflection amplitudes from a curved interface to that of a flat interface. For normal incidence, Hilterman (1975) gives:

$$CE = (1 + Z/A)^{-1/2} \tag{24}$$

where A is the radius of curvature of the bed and Z is the depth.

Shuey et al. (1984) extended this equation to the non-normal incidence case

$$CE(\Theta_1) = \left(1 + \frac{Z}{A_x \cos^2 \Theta_1}\right)^{-1/2}\left(1 + \frac{Z}{A_y}\right)^{-1/2} \tag{25}$$

where,

A_x = radius of curvature in x direction,
A_y = radius of curvature in y direction, and
Z = depth of crest of anticline or trough of syncline.

Note that the radii are negative for buried focus synclines and that Shuey's equation reduces to Hilterman's at normal incidence. Equation (25) indicates that the curvature effect (1) decreases with offset for an anticline, (2) increases with offset for a syncline with a focus above the surface, and (3) decreases with offset for a syncline with a focus below the surface. Macleod and Martin (1988) showed that DMO corrects the curvature effect.

Bernitsas (1990) extended Shuey's equation to the general case of three-dimensional curvature:

$$CE(\Theta_1) = (1 + Z/A_x)^{-1/2}(1 + Z/A_y)^{-1/2} \times \left[\frac{X^2}{Z(A_x + Z)} + \frac{Y^2}{Z(A_y + Z)} + 1\right]^{-1/2} \tag{26}$$

where X, Y, and Z are the spatial coordinates.

The effects of complex surface roughness have not been adequately investigated. Herman and Blonk (1990) suggest that surface roughness can be emulated by an appropriate transition layer.

As elucidated in Resnick et al. (1987), problems caused by dip include (1) errors in angle of incidence, (2) mixing information from different subsurface locations, (3) incorrect normal moveout, and (4) interference of mispositioned events.

The lensing effect of curved layers above the target are best compensated for by amplitude preserving prestack migration. Complex structure also commonly results in lateral overburden velocity gradients and associated AVO errors.

Geometrical Spreading

Newman (1973) gives the equations needed to correct for geometrical spreading. At normal incidence

$$D_o = tV_a^2/V_1, \tag{27a}$$

$$t_o = \sum t_i, \tag{27b}$$

and

$$V_a^2 = \sum t_i V_i^2/t_o \tag{27c}$$

where,

D_o = normal incidence geometric divergence,
V_1 = velocity in first layer,
t_o = zero-offset two-way reflection time,
t_i = interval two-way transit time of the ith layer,
V_a = time-weighted rms velocity, and
n = the number of layers i.

At non-normal incidence

$$D(\Theta_1) = \frac{(X^2 + 2X \sum d_i \tan^3 \Theta_i)^{1/2}}{\tan \Theta_1} \tag{28a}$$

and

$$X = 2 \sum d_i \tan \Theta_i \qquad (28b)$$

where,

$D(\Theta_1)$ = geometric divergence versus angle of incidence,
X = offset,
Θ_i = incidence angle in the ith layer, and
d_i = thickness of the ith layer.

Normal Moveout Errors

In order to measure the AVO on a sample by sample basis, it is necessary to perfectly correct the common depth point (CDP) gather for normal moveout (NMO) (Spratt, 1987; Swan, 1988). Conventional velocity analysis is generally not adequate to do the job and special care must be taken (Chiburis, 1984). Furthermore, as shown in Figure 13 (and Table 4), there is a fundamental ambiguity between stacking velocity and ODR (Spratt, 1987). NMO related problems are much less severe for methods which measure the energy within a window about the event of interest (Mazzotti, 1990) or for instantaneous AVO. Seismic modeling and waveform inversion can also be utilized to deal with the problem.

Overburden Effects

As transmission coefficients are angle dependent, the amplitude of the P-wave incident on the reflector of interest may also be angle dependent. This problem is most significant when the reflectivity above the target is very strong. Angle-dependent transmission losses are dependent on both the P-wave and S-wave velocity structures. Figure 14 and Table 5 show the effects of varying V_P and V_S over a particular target. Models A and B have the same V_P structure but different V_S structure. The reflection amplitudes are the same at near offset, but diverge significantly at far offsets. Similarly, models A and C have the same V_S structure but different V_P structures. The near-offset reflection amplitudes are very different, but the AVO is similar for both models. Figure 15 and Table 6 show that V_P/V_S variations in the very near surface can also significantly affect the AVO response. According to Gassaway (1984), transmission loss is the most signif-

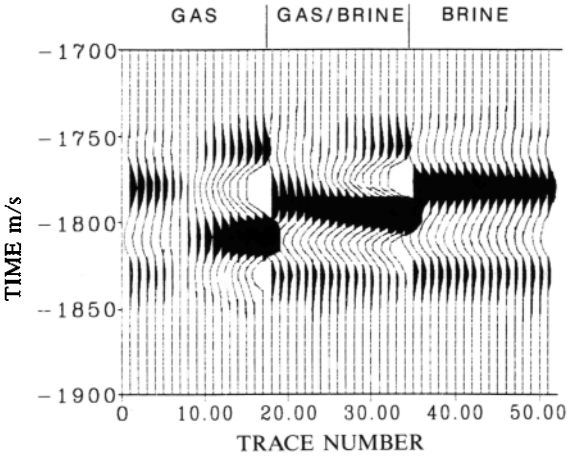

Fig. 13. Three NMO corrected synthetic CDP gathers for three models (A, B, and C) with identical P-wave velocity structure but differing S-wave velocity structures (see Table 4). V_P/V_S ratios are appropriate for gas sand (Model A), brine sand (Model C), and a sand with a gas-water contact (Model B).

Table 4. Model parameters for Figure 13.

Lithology	P-wave Velocity ft/s	P-wave Velocity m/s	S-wave Velocity ft/s	S-wave Velocity m/s	Density gm/cc	V_P/V_S	Thickness ft
Model A							
Shale	9000	2743	4575	1394	2.06	1.97	
Gas Sand	9300	2835	5782	1762	2.04	1.61	150
Shale	9000	2743	4575	1394	2.06	1.97	
Model B							
Shale	9000	2743	4575	1394	2.06	1.97	
Gas Sand	9300	2835	5782	1762	2.04	1.61	75
Brine Sand	9300	2835	4828	1472	2.08	1.93	75
Shale	9000	2743	4575	1394	2.06	1.97	
Model C							
Shale	9000	2743	4574	1394	2.06	1.97	
Brine Sand	9300	2835	4828	1472	2.08	1.93	150
Shale	9000	2743	4575	1394	2.06	1.97	

icant problem encountered in AVO analysis, and a layer stripping technique can be utilized to account for the overburden (see Figure 16).

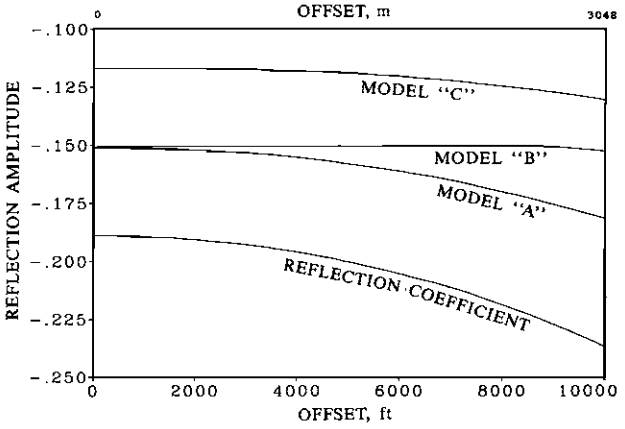

Fig. 14. Reflection amplitude variation with offset for three models (A, B, and C) with identical target reflection coefficient-versus-offset response but different overburden transmission losses (see Table 5). Model A has a shallow brine sand over the target gas sand. Model B shows the effect of increasing V_S in this layer, while Model C shows the effect of decreasing V_P.

Global transmission loss is very amenable to statistical correction. However, strong lateral change in overburden effects (as would result from shallow gas) is not easily corrected. Deterministic correction is problematical as the overburden cannot be perfectly characterized. Normalizing the measured AVO relative to a reference event is one way to tackle this problem (Chiburis, 1984 and 1987). The normalized AVO is given by

$$\frac{a(x)^{\text{tar}}/a_o^{\text{tar}}}{a(x)^{\text{ref}}/a_o^{\text{ref}}} \tag{29}$$

where $a(x)^{\text{tar}}$ and $a(x)^{\text{ref}}$ are the AVO for the target and reference events, respectively, and a_o^{tar} and a_o^{ref} are the normal incidence amplitudes. Troublesome variations in overburden can sometimes be detected by examining ties at line intersections (Huston and Backus, 1986).

Spatial variations in overburden velocities result in errors in the calculation of local angle of incidence which can be computed by ray tracing through a complex overburden. If the overburden can be represented by a linear velocity gradient

$$V_i = V_o + Kz \tag{30}$$

Table 5. Model parameters for Figure 14. * indicates the shallow layer for which the model parameters are varied.**

Depth ft	Depth m	Density gm/cc	*P*-wave Velocity ft/s	*P*-wave Velocity m/s	*S*-wave Velocity ft/s	*S*-wave Velocity m/s	V_P/V_S
Model A							
0	0	1.00	5000	1524	0	0	—
100	30	2.02	6000	1829	1326	404	4.52
1000	305	2.10	7000	2133	2188	667	3.20***
1200	366	2.18	8000	2438	3050	930	2.62
7000	2133	2.30	10000	3048	4774	1455	2.09
9000 (target)	2743	2.19	7161	2183	4774	1455	1.50
9100	2774	2.36	11000	3353	5636	1718	1.95
Model B							
0	0	1.00	5000	1524	0	0	—
100	30	2.02	6000	1829	1326	404	4.52
1000	305	2.10	7000	2133	4667	1422	1.50***
1200	366	2.18	8000	2438	3050	930	2.62
7000	2133	2.30	10000	3048	4774	1455	2.09
9000 (target)	2743	2.19	7161	2183	4774	1455	1.50
9100	2774	2.36	11000	3353	5636	1718	1.95
Model C							
0	0	1.00	5000	1524	0	0	—
100	30	2.02	6000	1829	1326	404	4.52
1000	305	2.10	3282	1000	2188	667	1.50***
1200	366	2.18	8000	2438	3050	930	2.62
7000	2133	2.30	10000	3048	4774	1455	2.09
9000 (target)	2743	2.19	7161	2183	4774	1455	1.50
9100	2774	2.36	11000	3353	5636	1718	1.95

where,

V_i = interval velocity,
z = depth,
V_o = velocity when $z = 0$, and
K is a constant, then (Ostrander, 1984)

$$\Theta_i = \tan^{-1}\,(zX + V_o X/K)/(z^2 + 2V_o z/K - X^2/4). \quad (31)$$

When velocities differ vertically or laterally from those used to compute angle of incidence, AVO errors will result (Xu and McDonald, 1988). When velocity increases with depth or decreases horizontally, an apparently bigger Poisson's ratio will be produced. The converse is also true.

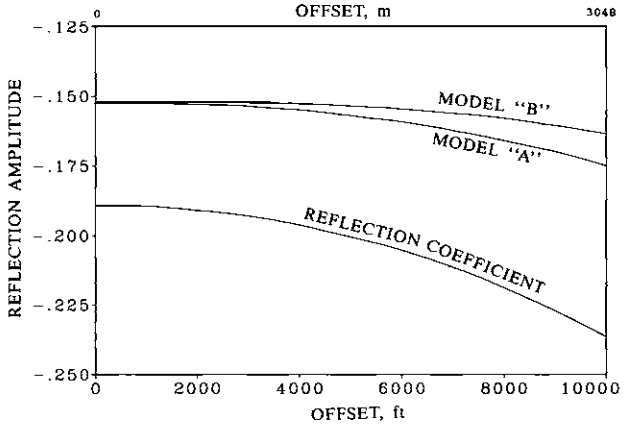

Fig. 15. Amplitude variation with offset for two models (A and B) with identical target reflection coefficient-versus-offset response but different overburden transmission losses (see Table 6). Model A has high near-surface V_P/V_S (wet sand) while model B has low near-surface V_P/V_S (dry sand).

Processing Considerations

Some conventional processing techniques are clearly only appropriate for relative AVO analysis: automatic gain control, whole trace equalization, non-amplitude preserving deconvolution or prestack migration, and all but the mildest velocity filtering. Muting may be too severe or not severe enough. Unrecorded processing gain adjustments can wreak havoc. Offset-dependent phase changes can result in incorrect stacking velocities and incorrect residual statics. NMO stretch increases the energy at far offsets and should be accounted for. Marine statics problems may obscure AVO responses (Treadgold et al, 1990b; Figure 17).

Duren (1990, 1991) applied the "range equation" to deterministically correct for "all AVO perturbing factors". The interpreter must keep in mind that such approaches can only be expected to apply a "ballpark" correction, and that significant residual problems must be expected.

Naive Application of Rock Physics Principles or Uncooperative Petrophysical Circumstances

According to Gassmann's equations, a gas sand with 1 percent gas saturation can have the same V_P/V_S as a commercial accumulation of gas. Thus, unless den-

Table 6. Model parameters for Figure 15.

Depth ft	Depth m	Density gm/cc	P-wave Velocity ft/s	P-wave Velocity m/s	S-wave Velocity ft/s	S-wave Velocity m/s	V_P/V_S
Model A							
0	0	2.00	5000	1524	550	168	9.09
100	30	2.02	6000	1829	1326	404	4.52
1000	305	2.10	7000	2133	2188	667	3.20
1200	366	2.18	8000	2438	3050	930	2.62
7000	2133	2.30	10000	3048	4774	1455	2.09
9000	2743	2.19	7161	2183	4774	1455	1.50
9100	2774	2.36	11000	3353	5636	1718	1.95
Model B							
0	0	2.00	5000	1524	3400	1036	1.47
100	30	2.02	6000	1829	1326	404	4.52
1000	305	2.10	7000	2133	2188	667	3.20
1200	366	2.18	8000	2438	3050	930	2.62
7000	2133	2.30	10000	3048	4774	1455	2.09
9000	2743	2.19	7161	2183	4774	1455	1.50
9100	2774	2.36	11000	3353	5636	1718	1.95

sity can be very accurately extracted utilizing far offset information, AVO cannot distinguish commercial and noncommercial gas accumulations. One wonders how many AVO failures were, in fact, technical successes where the "dry holes" actually contained small quantities of gas in the target zone.

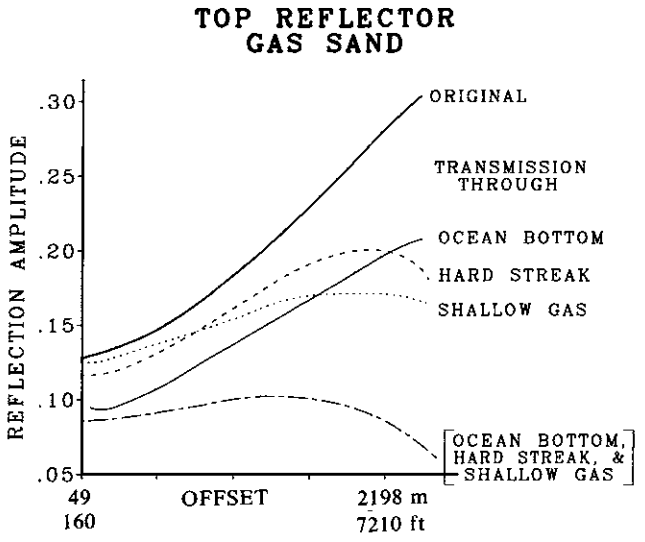

Fig. 16. Overburden transmission losses modify the target AVO. In this case, transmission through the ocean bottom, a hard streak, and a shallow gas sand suppresses the target gas sand amplitude increase with offset (from Gassaway, 1984).

Hilterman (1990) classified 5 different shale types with unique velocity-density trends. AVO response of a sand package depends on degree of shaliness and shale distribution within the package. Our petrophysical knowledge of shales remains inadequate.

According to Payne (1991): "Existing empirical relations do not provide S-wave velocity estimates with enough accuracy to yield quality model gathers." In light of the results of Greenberg and Castagna (1992), who showed S-wave velocity predictions arguably as good as direct S-wave sonic logs, one must ask if the direct "ground truth" is sufficiently adequate.

Hard sands and carbonates with strong frame moduli may show little gas effect. An unfortunate *fact of life* is the decreasing gas effect with increasing depth. However, gas brine contact reflections should be detectable in many instances.

Interpreters should also pay attention to expected Poisson's ratios for different lithologies. Abnormal AVO extracted Poisson's ratios (such as .49 for tight limestone) should be a warning flag that something is biasing the AVO analysis.

Inadequacies of the Forward Model

Wright (1984) concluded that anisotropy in overlying shales severely affects AVO (see Figure 18). The 20 percent P-wave anisotropy he assumed for shales seems somewhat extreme for the general in situ case,

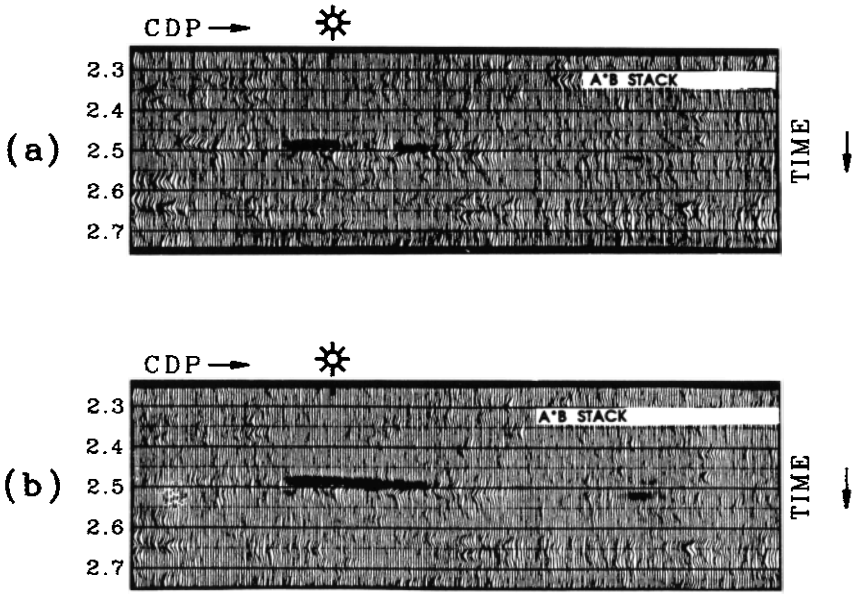

Fig. 17. A*B stack (normal incidence amplitude times AVO slope) before (a) and after (b) marine statics. A positive A*B stack indicates hydrocarbons in this case (from Treadgold et al., 1990a, b).

however, he points out that small amounts of gas in shales would increase anisotropy dramatically. This is a generally overlooked and perhaps very significant phenomenon. Anisotropy and attenuation can change the phase of the wavelet and can focus energy preferentially along the wavefront (Samec et al., 1990). Computing amplitudes within a small window about the event of interest, rather than on a sample by sample basis, will reduce this effect.

Inelastic attenuation and associated dispersion corrupt the AVO estimate (Luh, 1988). Overlying gas sands (which exhibit very high attenuation) can cause great difficulty. Q compensation and windowed amplitudes are recommended to combat this problem.

Theoretically, reflection amplitude at a porous interface is dependent on formation permeability (Stoll and Kan, 1981). However, Biot theory predicts a negligible permeability effect at seismic frequencies (Dutta and Ode, 1983).

For very shallow targets the plane-wave assumption may not be valid (Krail and Brysk, 1983; Rendleman and Levin, 1988; Wapenaar et al., 1990).

Interpretation Considerations

The interpreter must weigh all these complications while synthesizing additional dimensions of data. Consequently, the handling and display of the additional offset data becomes a major problem. Polarity remains an issue, as hard streak AVO can be mistaken for gas sand AVO when polarity is reversed. Gas leakage over the reservoir (Sengupta and Rendleman, 1989) can confound AVO analysis in a variety of ways: increased scattering, attenuation, and anisotropy and decreased P-wave velocity and V_P/V_S over the target. Finally, vertical and lateral resolution limits and variable S/N for various extracted quantities must be kept in mind.

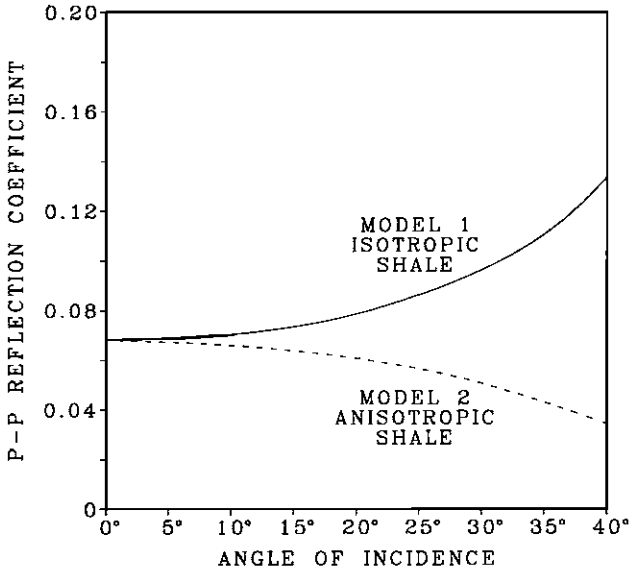

Fig. 18. Reflection coefficient versus offset for a shale/sand interface. Model 1: isotropic shale. Model 2: anisotropic shale (from Wright, 1984).

SEISMIC DATA PROCESSING FOR AVO ANALYSIS

When attempting to select an appropriate data processing scheme for AVO analysis, the processor must carefully balance two competing objectives: (1) Noise suppression and isolation of the reflectivity of the event of interest, versus (2) not biasing or otherwise corrupting the reflectivity variation with offset. This tradeoff usually leads to the selection of a basic but robust processing scheme (Ostrander, 1984; Chiburis, 1984; Long and Richgels, 1985; Yu, 1985; Dey-Sarkar and James, 1986; Fouquet, 1990). Keep in mind that the processor is deprived of his strongest weapon; CDP stacking. Table 7 gives some processing schemes presented in the literature.

In areas of significant dip or structural complexity, we are forced to utilize more sophisticated processing techniques. Resnick et al. (1987) and de Bruin et al. (1988, 1990) handle complex surfaces by prestack migration. Amplitude preserving prestack migration is recommended for all AVO projects. The use of Radon transform techniques for multiple suppression is also highly recommended (Kelamis et al., 1990). Resnick (1988) asks the important question: "When have we overprocessed the data?"

"Weighted-stacking" (Smith and Gidlow, 1987) is a means of reducing prestack information to AVO attribute traces (usually some form of Shuey's coefficients) versus time. This is accomplished by computing the local incident angle for each time sample and then performing regression analysis to solve for the first two or all three coefficients of an equation of the kind

$$R_{PP}(\Theta_1) \approx A + B \sin^2 \Theta_1 + C \sin^2 \Theta_1 \tan^2 \Theta_1. \quad (32)$$

A is the "zero-offset" stack or "true" normal incidence reflectivity, B is commonly referred to as the AVO "slope" or "gradient". Following Smith and Gidlow (1987), we have from Wiggins (1983)

$$\Delta V_S/V_{Sa} = A - B \quad (33)$$

where $\Delta V_S = V_{S2} - V_{S1}$, and $V_{Sa} = (V_{S2} + V_{S1})/2$. Using Gardner's relation:

$$\Delta\rho/\rho_a \approx .25\ \Delta V_P/V_P \quad (34)$$

where $\Delta V_P = V_{P2} - V_{P1}$, and $V_{Pa} = (V_{P2} + V_{P1})/2$. We also have:

$$\Delta V_P/V_{Pa} \approx 8A/5. \quad (35)$$

Smith and Gidlow (1987) define the "fluid factor", ΔF, as the difference between observed $\Delta V_P/V_{Pa}$ and $\Delta V_P/V_{Pa}$ predicted from $\Delta V_S/V_{Sa}$. Using the "mudrock trend" (Castagna et al., 1985) they get:

$$\Delta F = \Delta V_P/V_{Pa} - 1.16(V_S/V_P)\Delta V_S/V_{Sa} \quad (36)$$

where V_S/V_P is the background S-wave to P-wave velocity ratio which can be predicted by application of the mudrock trend to interval velocities obtained from conventional velocity analysis. Of course, when necessary, a locally calibrated V_P versus V_S trend can be employed. An empirically derived function from the AVO data which usually does not match the petrophysical control is often used. This is necessitated by the biases in the seismic data resulting from the myriad of complicating factors discussed in the preceding section. Figure 19 shows $\Delta V_P/V_{Pa}$, $\Delta V_S/V_{Sa}$, $\Delta\sigma/\sigma_a$, and ΔF displays for a real data example (Smith and Gidlow, 1987). ΔF shows distinct anomalies which are not obvious on the other sections. Advantages and disadvantages of weighted stacking are listed in Table 8 (Lortzer et al., 1988).

INTERPRETATION OF AVO DATA

Gas Detection

By far, gas-sand detection is the most promising application of AVO analysis. It is hoped that the characteristically low V_P/V_S of gas sands should allow their differentiation from other low impedance layers such as coals and porous brine sands. Rutherford and Williams (1989) define three distinct classes of gas sand AVO anomalies (see Figure 20). Class 1 occurs when the normal incidence P-wave reflection coefficient is strongly positive and shows a strong amplitude decrease with offset and a possible phase change at far offset. Class 2, for small P-wave reflection coefficients, shows a very large percentage change in AVO. If the normal-incidence reflection coefficient is slightly positive, a phase change at near or moderate offsets will occur. Class 3 anomalies have a large negative normal-incidence reflection coefficient which becomes more negative as offset increases (these are classical bright spots). A simple rule of thumb which generally applies to shale over gas sand reflections: the reflection coefficient becomes more negative with increasing offset.

The literature is rich in gas sand detection examples from a variety of localities: the Sacramento Valley (Ostrander, 1984; Gassaway, 1984; Soroka et al., 1990;

Table 7. Processing schemes reported in the literature.

Ostrander, 1984:	1. spherical divergence correction 2. exponential gain correction 3. minimum-phase spiking deconvolution 4. velocity analysis 5. NMO correction 6. trace equalization 7. horizontal trace summing
Chiburis, 1984:	1. mild *f-k* multiple suppression 2. spherical divergence and NMO correction 3. whole-trace equalization 4. flattening on a consistent reference event 5. horizontal trace summing 6. peak amplitudes picked interactively 7. smoothed least-squares curve fitting 8. despiking of outliers 9. curve refitting 10. results clipped and smoothed
Long and Richgels, 1985:	1. spherical divergence, attenuation, and emergence angle corrections determined by regression analysis 2. variations in source strength, receiver sensitivity, overall offset amplitudes, consistently modelled and resolved 3. deviations rejected as noisy 4. inverse amplitude correction 5. spectral surface array attenuation correction 6. accurate NMO applied using very fine velocity sampling and geologically consistent velocity contouring 7. surface consistent deconvolution for land data 8. CDP residual statics carefully monitored for incorrect shifts due to AVO effects 9. minimal muting 10. common offset spatial filtering 11. linear or non-linear fit for AVO coefficients
Yu, 1985, a and b:	1. apply exponential gain, suppress coherent noise, and remove gain 2. offset compensation 3. deconvolution, 4. NMO correction 5. surface consistent correction 6. partial trace sum 7. bandpass 8. section dependent equalization
Todd, 1986:	1. spatial averaging 2. gapped deconvolution 3. geometrical divergence correction 4. global velocity analysis and NMO correction 5. partial stacking 6. correction for average amplitude variation in time and offset

Gabay, 1990), the North Sea (Wrolstad, 1986; Snyder et al., 1989, Strudley, 1990), the Gulf Coast (Zilik, 1989; Hoopes and Aber, 1989; Burnett, 1989 and 1990; Rutherford and Williams, 1989), offshore Gulf of Mexico (Ostrander, 1984; Rutherford and Williams, 1989, Zimmerman and Fahmy, 1990), the Arkoma Basin (Rutherford and Williams, 1989), the Arabian Gulf (Chiburis, 1984; 1987), Alaska (Zimmerman and Fahmy, 1990), and Italy (Mazzotti, 1990). Notably, Soroka et al. (1990) claim a 90 percent success ratio with three dimensional (3-D) AVO in the Sacramento Valley. Similarly, in the Sacramento Valley, Gassaway (1984) was successful in predicting hydrocarbons 13 out of 15 times, and in predicting no hydrocarbons 8 out of 12 times. Table 9 shows the AVO track record in a particular Gulf Coast field (Burnett, 1990).

Successful hydrocarbon detection in carbonates has also been reported (Chiburis, 1987). Based on petrophysical arguments, we expect this to be possible only for restricted circumstances when the carbonate rock frame is sufficiently compressible for the fluid modulus to significantly influence the bulk modulus of the saturated rock. This would require significant amounts of low aspect ratio porosity. For porous high aspect ratio carbonates, it may be possible to exploit the effect of gas on bulk density.

Enhanced Oil Recovery Monitoring

As shown in Ito et al. (1979) and others, the effect of steam on rock V_P/V_S is very similar to the effect of

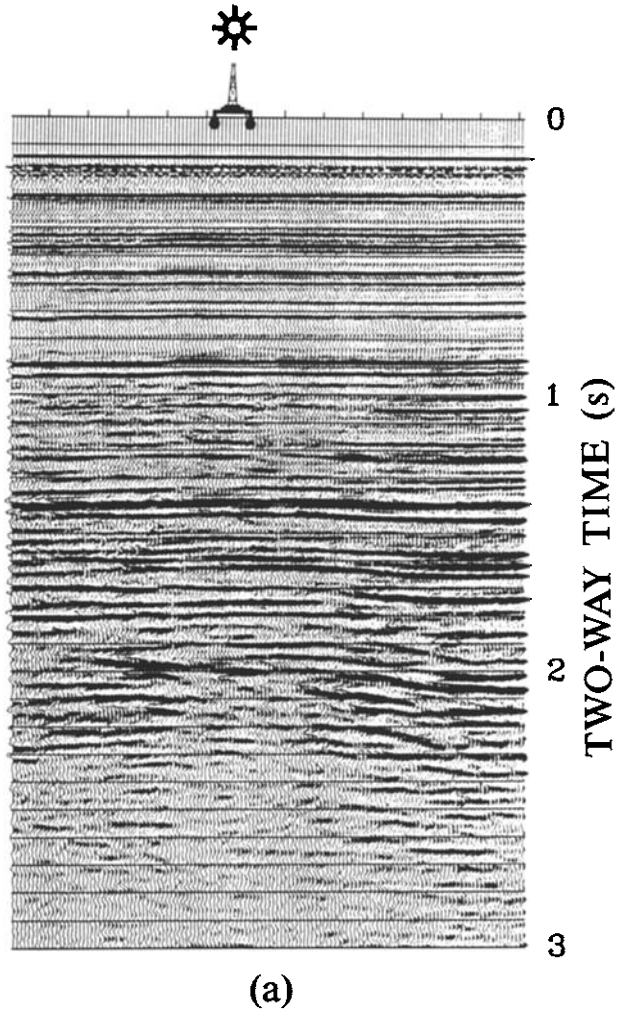

Fig. 19. Weighted stack outputs. (a) $\Delta V_P/V_{Pa}$, (b) $\Delta V_S/V_{Sa}$, (c) $\Delta\sigma/\sigma_a$, and (d) ΔF (from Smith and Gidlow, 1987).

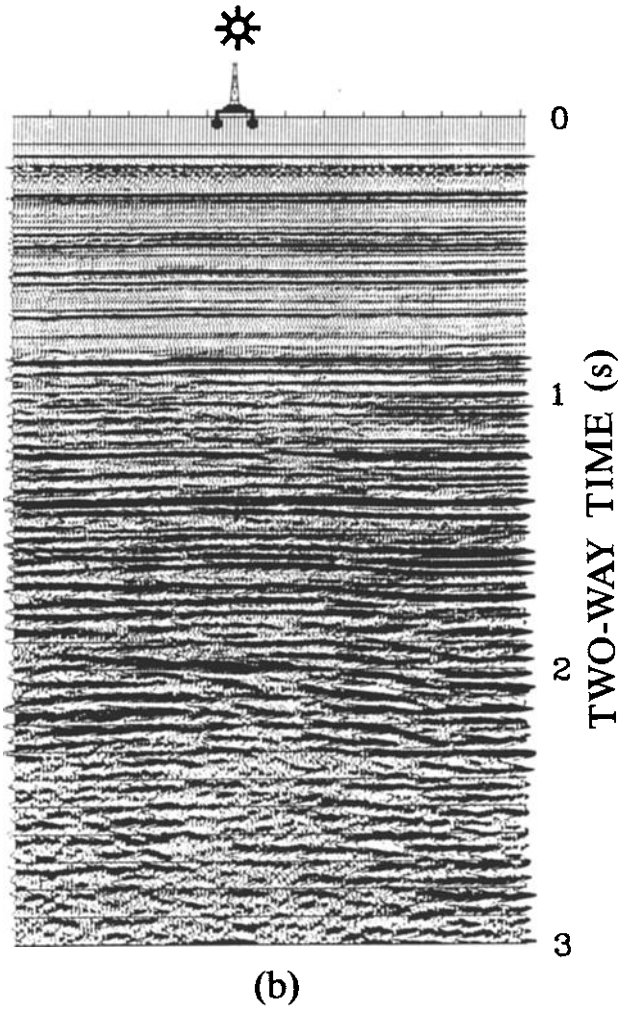

Fig. 19. continued

natural gas. Tsingas and Kanasewich (1991) showed that AVO can be very effective for monitoring steam flooding. As seismic is acquired at various stages of enhanced oil recovery (EOR), many of the perturbing factors we have discussed remain constant and cancel out when the AVO measurements are ratioed. This application utilizes reflection seismology's greatest strength; the ability to detect changes. Other EOR processes (such as water flooding), although more subtle in effect, may also be amenable to AVO analysis.

Oil Detection

Hwang and Lellis (1988) describe bright spots due to high gas-oil-ratio (GOR). A detailed review of factors affecting the acoustic properties of oils is presented in Castagna et al., this book pages 135–171 (1993). Under favorable circumstances, oil sands can exhibit V_P/V_S ratios about half-way between brine and gas sands. Gassaway (1984) and Chiburis (1987) report successful utilization of AVO to detect oil reservoirs.

Lithology Identification

The petrophysical "signal" for AVO lithology analysis is the lithology dependence of V_P/V_S. Inspection of V_P versus V_S trend curves for sandstones, shales, limestones, and dolomites, reveals that lithology discrimination is most robust at higher velocities where sandstones have low V_P/V_S (1.5–1.6) and the other lithologies have higher V_P/V_S (1.7–2.0). Some examples from the literature include Johnson (1988; sands versus carbonates), Fuller et al. (1989; sand versus

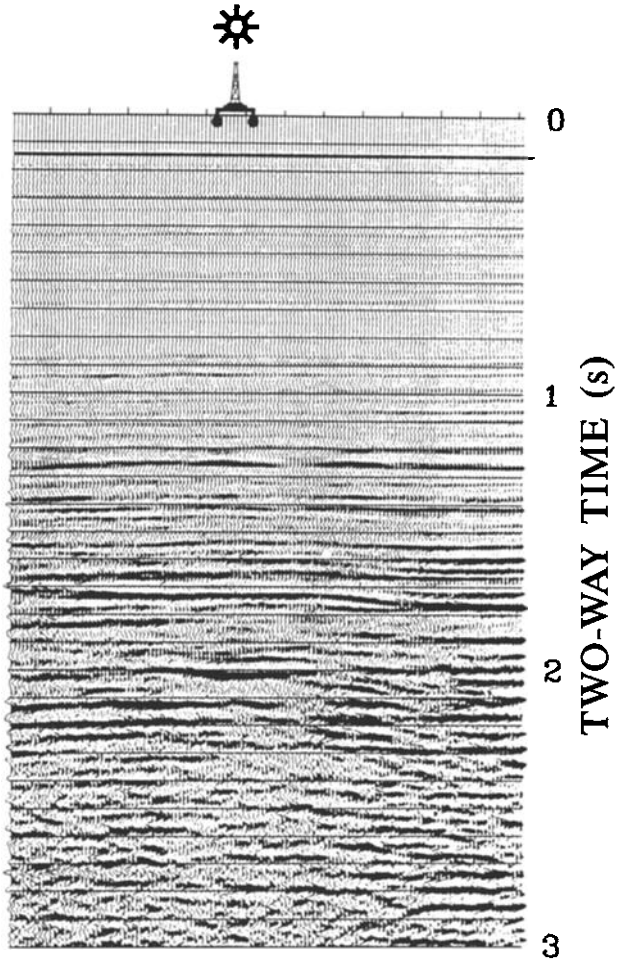

(c)

Fig. 19. continued

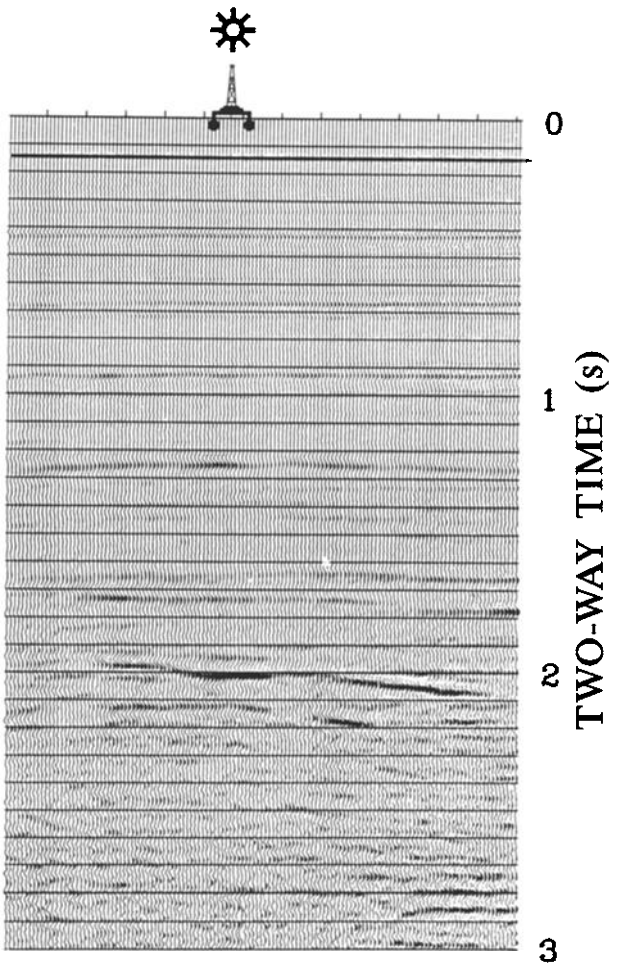

(d)

Fig. 19. continued

shale), Ramirez (1990; salt versus clastics), and Mazzotti (1984; high-velocity layers in general).

Porosity Identification

AVO can be used to detect porosity in carbonates (Chacko, 1989; Pigott et al.; 1990). Given the highly variable pore structure of carbonates, it is difficult to make generalizations regarding expected AVO response without local calibration. Usually V_P/V_S is insensitive to porosity and pore fluid content (with the sometimes important exception of unconsolidated carbonate sands or lithified carbonates with flat pores or microfractures). For vuggy porosity dominated by equant (spherical) pores, density may be the parameter which is most sensitive to porosity and pore fluid content; density becomes even more important when the rock has variable clay content. In these cases, Shuey's third coefficient (C) may be required to separate velocity and density contrasts.

Land Versus Marine AVO

One would expect, given the data quality concerns for land seismic profiles, that AVO would be primarily applied offshore. In fact, severe short period multiple problems may make marine data quality no better for AVO analysis than land data in many cases. Ostrander's original paper showed successful onshore examples. The Sacramento Valley, in particular, has yielded a plethora of successful AVO analyses (Ostrander, 1984; Gassaway, 1984; Gabay, 1990; Soroka et al., 1990; and various papers in this volume). The success ratio of AVO in the Yegua trend is a reported 80 percent (Allen, personal communication).

Table 8. Advantages and disadvantages of weighted stacking methods (after Lortzer et al., 1988).

Advantages:
(1) fast
(2) no local minima
(3) wavelet not required
(4) "zero offset stack" more accurate than conventional stack
Disadvantages:
(1) outputs relative parameters only
(2) wavelet is not removed
(3) sensitive to NMO errors
(4) output density and velocity contrasts are not independent
(5) shear and V_P/V_S contrasts and fluid factor are noisy measurements

Table 9. Crosstabulation of well cumulative production versus AVO effect, Mestena Grande Field, Jim Hogg Co., Texas (from Burnett, 1989 and 1990). The AVO effect is defined as follows: Strong = high amplitude which increases with offset, Moderate = medium amplitude which varies little with offset, Weak = low amplitude which decreases with offset.

Cumulative Production	AVO Effect Strong	Moderate	Weak
1–4 BCF	5	1	0
Less than 1 BCF	0	3	2
abandoned	0	1	3

Interpretation Techniques

AVO analysis brings additional dimensions to the seismic interpretation problem. Uniqueness of the result is less important than the need to provide AVO information to the interpreter in a manageable form. Onstott et al. (1984) stated the problem very well: "The one-dimensional seismic inversion problem has not been solved perfectly and never will be. Nevertheless, seismic interpreters do a reasonable job of inferring subsurface structure and lithology from CDP

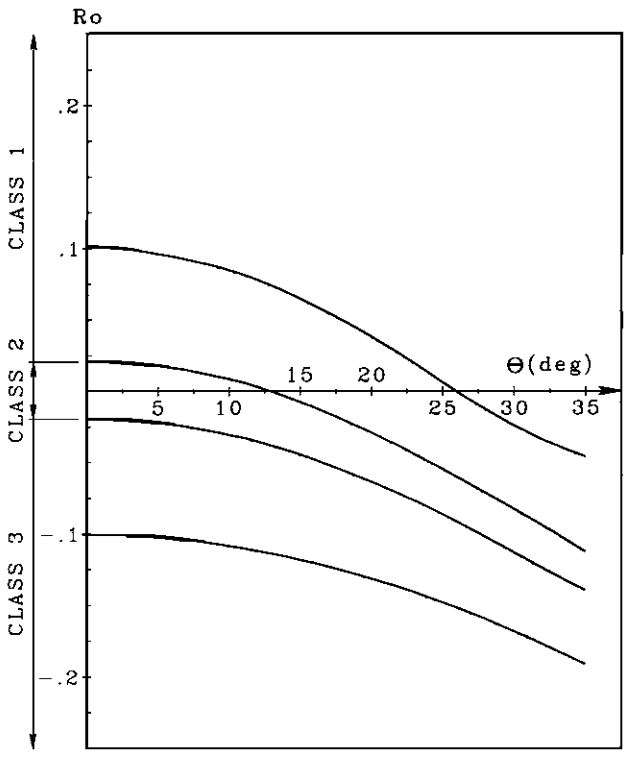

Fig. 20. Zoeppritz P-wave reflection coefficients for a shale over gas sand interface for a range of R_P values. The Poisson's ratio and density were assumed to be .38 and 2.4 gm/cc for shale and .15 and 2.0 gm/cc for gas sand (from Rutherford and Williams, 1989).

stack sections by applying knowledge and intuition. The same can be done, with more accurate results, from reflectivity-versus-offset sections, provided that an organized method of interpretation is developed." Toward this end, a variety of interpretive displays have been devised (see Table 10).

Full elastic-wave modeling techniques are described elsewhere in this volume. A simple and easy modeling technique is to calculate the AVO gradient B as a function of depth from well log data, and to convolve the B series with a wavelet. Johnson (1988) shows an excellent use of the B synthetic (see Figure 21).

Partial near, middle, and far offset range stacks simply and robustly show AVO variation in interpretable form (Onstott, 1984, see Figure 22; Todd and Backus, 1985). Figure 23 shows a partial stack display for a class II AVO anomaly (Rutherford and Williams, 1989). In certain circumstances, the partial stack may have better S/N than the full CDP stack (Todd, 1986). Plane-wave decomposition may be used to produce common ray parameter stacks. The colorstack (Onstott, 1984) superimposes near, middle, and far offset ranges; each range represented by a different color. Amplitudes are represented by color intensity and the partial stacks are superimposed. The result is a multicolor seismic section which reveals the amplitude variation with offset; the dominant color indicating the offset range with the greatest amplitude. A "white" result indicates constant amplitude with offset. The method also provides an excellent means of NMO quality control, as imperfectly aligned events show a distinct color fringing. The colorstack, with the help of the human eye, allows full exploitation of the key piece of AVO information which ". . . is the *difference* in AVO behavior along a seismic line when moving off a structure containing hydrocarbons" (Chiburis, 1987).

Table 10. Listing of AVO interpretation displays (after Wrolstad, 1988; and Nelson, 1989)

Raw CDP gathers
AVO processed and NMO corrected CDP gathers
Crossplot of event amplitude or energy versus offset
Common offset stack
Partial stack
Prestack difference gathers at line intersections
P-wave reflection coefficient (normal incidence; R_p or "A")
S-wave reflection coefficient (normal incidence; R_s)
Difference between P and S reflection coefficients ($R_P - R_S$)
Gradient stack (also called "B" stack or "AVO slope")
Product of P-wave reflection coefficient and AVO slope (A*B)
Colorstack
Change in Poisson's ratio section ($\Delta\sigma$)
Envelope of $\Delta\sigma$
Color enveloped $\Delta\sigma$
Fluid factor (ΔF)

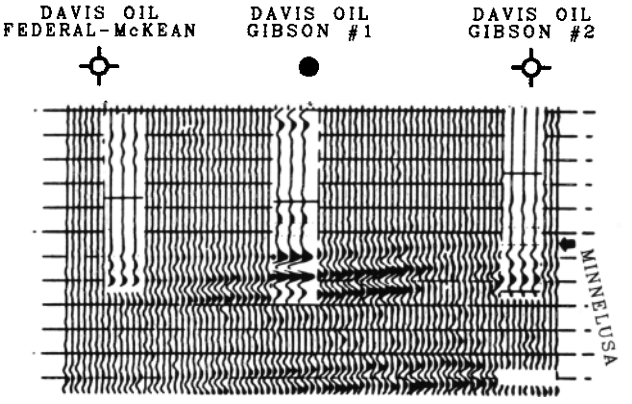

Fig. 21. AVO gradient (B) processing and modeling (from Johnson, 1988).

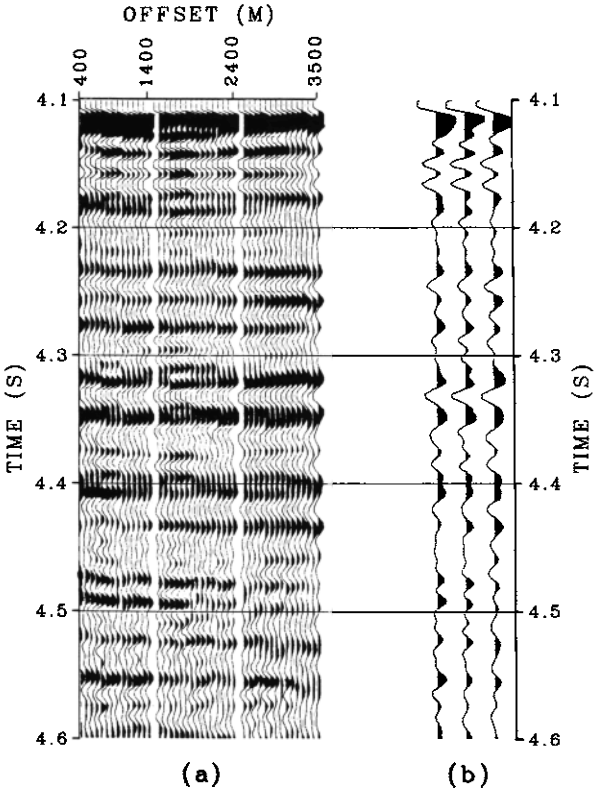

Fig. 22. (a) A portion of a normal moveout corrected common depth point gather divided into three offset ranges. (b) Partial stack traces formed by summing traces within the indicated offset ranges (from Onstott, 1984).

ELASTIC INVERSION

Seismic inversion is the construction of an earth model which is compatible with observed seismic data on the basis of an assumed functional relationship (forward model) between the earth model and "perfect" (noise free) data. It is interesting to note that conventional seismic interpretation is, by this description, a form of seismic inversion. In general, although the functional relationship is nonlinear, the inverse problem is linearized, and an iterative approach is used.

Given infinite computer time, one could model a very large number of combinations of V_P, V_S, ρ, and Q profiles. A combination of these parameters which results in acceptably small discrepancy between real and synthetic data would be taken as the inverted earth model. The objective of seismic inversion is to arrive at an adequate earth model with a limited number of iterations. This is often accomplished by starting with an initial guess and then converging to a solution by minimizing the error seismograms.

Elastic inversion of an entire CDP gather has several advantages over conventional AVO methods such as the weighted stack: (1) The wavelet is removed and interfering reflections are deciphered; tuning is no longer a fundamental limitation. (2) Differential NMO, mode conversions, and multiples become signal rather than noise, and (3) A priori information in the form of starting models and constraints of various kinds can be incorporated, thereby improving effective S/N and bandwidth.

Seismic inversion has the fundamental problem of nonuniqueness and the major disadvantage of high computer costs. It is likely that "automated" modeling, where inverse theory will guide the interpreter in refining his model, will emerge in the near future as a practical tool.

Mora (1984, 1986, 1987a, 1987b, 1987c, and 1988) illustrates elastic earth model reconstruction by full-waveform inversion. For land data, strong singly converted S-waves help to constrain the inversion. Approaches that fix the background velocity (Stolt and Weglein, 1985) will exhibit wild fluctuations if valid velocity-density relationships are not employed (Backus, 1987).

Inversion approaches that depend on amplitude only (Parsons, 1986; Gelfand et al., 1986; etc.) though computationally more acceptable at the present time, should be less reliable than full-waveform techniques which utilize time and moveout information.

Hampson and Russell (1990) combat the nonuniqueness problem by using a Monte Carlo approach, where

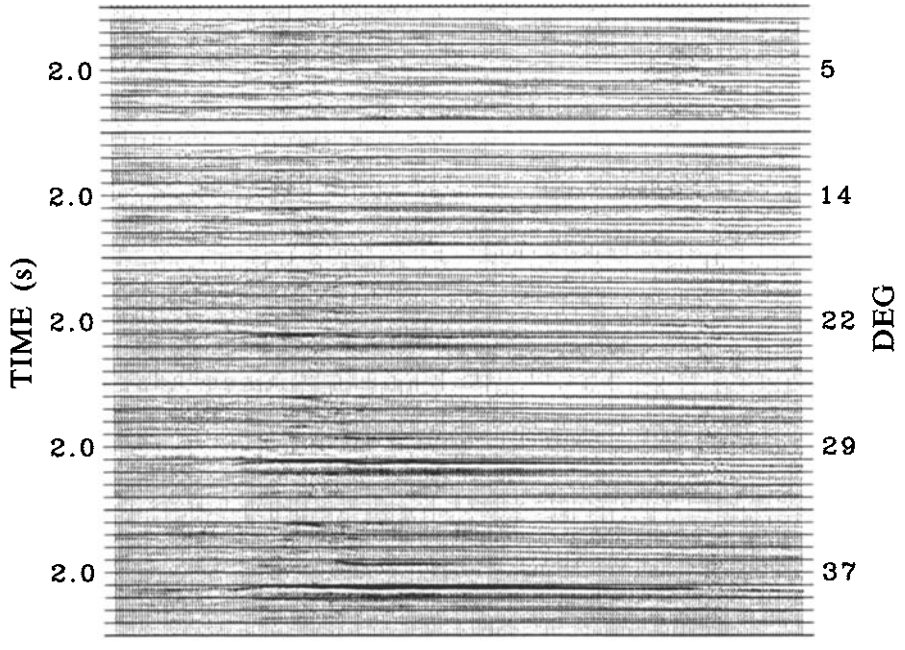

Fig. 23. Panel display of constant reflection angle sections. The angles posted on the right side of the figure refer to the centers of the reflection angle ranges in each panel. Each panel displays 1.6 to 2.4 s (from Rutherford and Williams, 1989).

a variety of starting models are randomly generated. Given enough starting models (and sufficient computer time) this approach can circumvent "local minima" to some extent. However, it is difficult to assess what constitutes "enough" starting models.

Carrazzone and Srnka (1989) and Assous and Richard (1989) have reported excellent headway in full-gather inversion. Tarantola et al. (1990) review the current state-of-the-art. Ultimately, inversion may yield four images of the subsurface: low frequency V_P and V_S, and high frequency P-wave and S-wave impedance. There is ambiguity between low-frequency P-wave velocity and high-frequency impedance. Further ambiguity results from attenuation, anisotropy, and wavelet uncertainty.

Increased inversion stability and robustness can be achieved if multicomponent data are available (Berkhout and Wapenaar, 1988; Lortzer and Berkhout, 1989; Tarantola et al., 1989; de Haas and Berkhout, 1989; Du and Spencer, 1990; Wang et al., 1990; among others).

Pan et al. (1990) studied the sensitivity of target-oriented full-waveform inversion. They found that pay thickness estimates for shallow gas sands were robust, even at thicknesses below 1/10th of a wavelength and in the presence of coherent noise (except at the tuning thickness; see Figure 24). The problem at tuning is attributed to the amplitude and time-thickness insensitivity which occurs on a Widess (1973) tuning plot at the tuning thickness. The pay thickness can be estimated (but not resolved) well below tuning from the inverted Poisson's ratio of an interval of which only a fraction is gas pay. Figure 25 shows a crossplot of inverted Poisson's ratios and P-wave impedances for a shallow gas prospect. A priori, we expect gas sands to have Poisson's ratios of about .1 and brine sands and shales to have Poisson's ratios above .4 in this locality. To the contrary, a continuum of Poisson's ratios are observed. This is attributed to intervals which are not entirely gas pay; these would exhibit a composite Poisson's ratio averaged in some way between gas sand and brine sand or shale. By assuming a time-average relationship for the layers for which the composite Poisson's ratio has been inverted and utilizing á priori V_P versus V_S trends, and Gassmann fluid substitution, the fractional gas sand thickness within each composite layer can be computed (the net thickness is determined—not the distribution). For the special case of a sand interval with S-wave velocities about equal above and below the gas/water contact and known average velocities for the gas and water-saturated intervals, the fractional gas sand thickness, X_{gas}, can be extracted from the inverted V_S/V_P by:

$$X_{\text{gas}} = \frac{1/V_P^{\text{br}} - (V_S/V_P)/V_S^{\text{br}}}{1/V_P^{\text{br}} - 1/V_P^{\text{gas}}} \tag{37}$$

where,

V_P^{br} = brine-sand P-wave velocity,
V_P^{gas} = gas-sand P-wave velocity, and
V_S^{br} = brine-sand S-wave velocity.

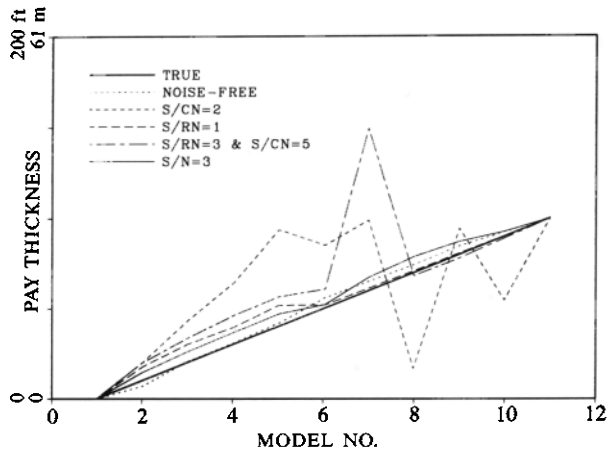

Fig. 24. Inverted gas sand pay thickness estimate for noise-free synthetic data, and data with added random and coherent noise (from Pan et al., 1990). CN = coherent noise. RN = random noise.

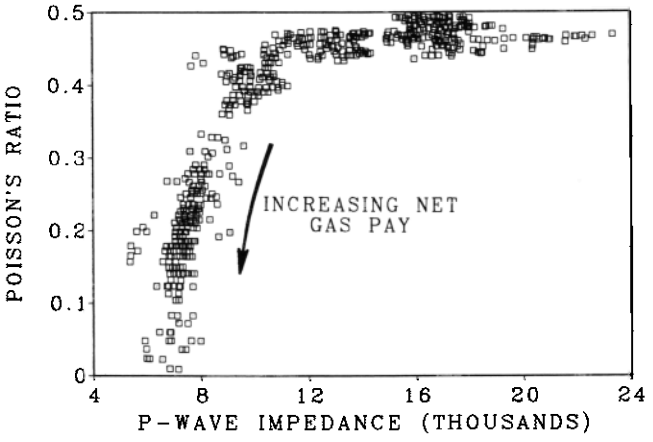

Fig. 25. Inverted Poisson's ratio versus inverted P-wave impedance in the vicinity of a shallow Gulf of Mexico bright spot. For this situation Poisson's ratios of about .1 are expected for gas sands and .4 or above are expected for brine sands and shales. Intermediate Poisson's ratios are caused by vertical averaging of thin layers.

As V_S/V_P is one of the more robust parameters obtainable from AVO data, the predicted X_{gas} is also robust, providing the above assumptions are valid. Figure 26 is a crossplot of observed versus predicted gas thicknesses for some shallow Miocene Gulf of Mexico sands. (Thanks to Al Garcia and Chi Young who performed the inversions). Please note that the two points with no sand present are localized "shale-outs" (verified by side-tracking) which are believed to be smaller than a Fresnel zone.

This example demonstrates the power of a priori constraints tied to borehole information. Such inversion schemes are probably most applicable in the vicinity of well control.

MULTICOMPONENT AVO

Multicomponent seismology and AVO analysis are intimately linked through the Zoeppritz equations. A review of multicomponent analysis techniques is beyond the scope of this book (the reader is referred to Danbom and Domenico, 1986).

Garotta and Granger (1987), and Miles and Gassaway (1989) among others have demonstrated the utility of combined AVO analysis of P, S_V, and S_H data. A few key points follow:

(1) Inversion of the Zoeppritz equations is unique for S_H-waves (Rosa, 1976).

(2) The slope of converted P to S_V-wave AVO is primarily dependent on the S-wave impedance contrast.

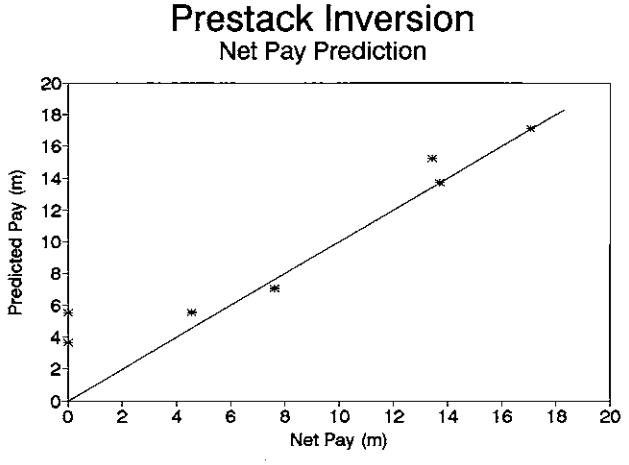

Fig. 26. Calculated net gas sand thickness versus observed net gas sand thickness. The erroneous sand thicknesses at zero observed net pay are localized shale outs smaller than a Fresnel zone (verified by further drilling).

(3) S-waves are less perturbed by transmission through overlying gas sands than are P-waves.

(4) The redundancy of multicomponent AVO measurements is advantageous. This is readily apparent from the following analysis (Corrigan, personal communication). Let us represent the converted P to S_V-wave AVO by:

$$R_{PS} \approx G \sin^2 \Theta_1 \tag{38}$$

where R_{PS} is the incident P-wave to reflected S_V-wave reflection coefficient. Remembering,

$$R_{PP} \approx A + B \sin^2 \Theta_1 \tag{39}$$

it can be shown (for $V_P/V_S \approx 2$) that

$$G \approx B - A \tag{40}$$

(5) Additional S-wave information such as reflection time ratios, normal incidence amplitude ratios, and S-wave moveout further constrains the analysis (Garotta, 1988).

OTHER APPLICATIONS

We have concentrated on the "seismic lithology" aspects of AVO analysis. In fact, comprehension of AVO effects leads to generally better data processing and interpretation and some unique applications in special circumstances.

Effects of AVO on Conventional Interpretation

When sands and shales have about the same impedance, sand-shale reflections may be weak at near offsets, and strong at far offsets. This variation will produce events on the stacked section which cannot be modeled with a simple normal incidence synthetic seismogram and is explained by the following argument: Consider a sand-shale interface. If impedance is constant across the interface, then velocity-density relationships tell us that the shale density should be greater than the sand density and the shale P-wave velocity should be less than the sand P-wave velocity. Using the mudrock V_P versus V_S line (or more precise sandstone and shale trends), it can be shown that the shale will have lower S-wave impedance and higher V_P/V_S than the sandstone. The V_P/V_S drop across the interface will result in the reflection coefficient becoming more negative with offset. As the reflection coefficient is near zero at normal incidence, it should be negative at far offsets. The stacked trace will show a relatively strong negative event.

Wrolstad (1986) showed a comparison of real North Sea seismic data with an elastic prestack synthetic gather computed with predicted S-wave velocities. A

stack of the prestack synthetic shows a significantly better tie to the stacked field data than does the conventional synthetic seismogram.

In general, conventional synthetic seismograms should be augmented with synthetic prestack gathers, and the seismogram produced by stacking the synthetic prestack gather.

AVO Effects in Data Processing

It is well recognized that amplitude and phase variations versus offset may cause CDP stacking to degrade reflection data quality (Poley et al., 1989). Extraction of the "A" term by least squares regression produces a "zero offset" stack (Denham et al., 1985; Coruh and Demirbag, 1989, and Kolb et al., 1989). As elucidated in Denham et al. (1985), the zero-offset stack provides: (1) a better approximation to the normal incidence P-wave reflection coefficient, (2) broader bandwidth and higher frequencies, and (3) higher resolution. Noise can be combatted by restricting the rate-of-change of the AVO slope, thereby stabilizing the A term extraction. Seismic impedance traces inverted from zero-offset stack traces should be superior to conventional seismic impedance logs.

Varying reflection-coefficient-versus-offset also contradicts the assumptions of conventional velocity analysis (see Figure 14). In clastic sections exhibiting a well-defined V_P versus V_S relationship, it may be possible to improve velocity analysis using a model-based approach; this is a variation of full gather inversion, however, V_P is the only unknown parameter while V_S and ρ are specified as functions of V_P. Large residuals caused by gas sands would indicate a need to change the V_S and ρ functions.

Critical Angle Effects

The amplitude build up at critical angle for positive reflections can be used to identify polarity, as this amplitude increase does not occur for negative reflections, and to illuminate very weak reflectors at the critical angle (Anstey, 1977). Makris and Thiessen (1984) use critical reflections to image through high velocity evaporites. In some cases, the large amplitude build up can be used to determine the critical angle. Chiburis and Al-Faraj (1987) determined the critical angle in this way and then applied Snell's law to extract overburden velocity and reflector depth.

FUTURE DIRECTIONS

Successful AVO analysis requires a degree of integration beyond that which has been absolutely necessary for conventional seismic interpretation: well logging, rock physics, reservoir engineering, seismic data acquisition and processing, seismic modeling and inversion, conventional seismic interpretation, and a healthy dose of geological concepts and constraints must be incorporated into the analysis. A formula for failure is to couple these disciplines in a straight-line cascaded series of boxes: be they computer programs, departments, or experts. These disciplines must be intimately interwoven in the mind of the interpreter and in the form of truly integrated workstation software. Recent developments in computing hardware and software have brought us to the threshold of realizing this goal; however, as of this writing, no single software package can do all aspects of the job adequately. Sumner (1988) provides an excellent discussion in the area of AVO technology transfer.

The ongoing revolution in computing essentially guarantees significant improvement in AVO analysis. Workstation technologies allow the interpreter to effectively deal with more kinds and dimensions of data. Increased memory, computation speed, and storage capacity means there will be more channels, longer spread lengths, more 3-D data, better processing, more sophisticated modeling, and more ambitious inversion schemes. Expert systems will assist the interpreter in those disciplines in which he or she is not well versed, and will also provide localized expertise for particular areas or formations.

With the increasing computation speed and memory becoming available, AVO inversion techniques are becoming practically applicable. Appropriate selection of parameters, background velocity, wavelet estimation, application of a priori information, and methods for interpreter interaction are still important issues which remain to be resolved. We should not let nonuniqueness in AVO inversion blind us to the tremendous utility of AVO analysis in general. After all, let us not forget that generating structure maps from reflection times is an inherently nonunique process. Ultimately, geophysics is a science of anomalies, and anomalies are defined by our expectations. There is no rigorous solution and our expectations are inexact; nevertheless, AVO does have the ability to reduce risk and to "illuminate" new prospects which were previously overlooked.

ACKNOWLEDGMENTS

Special thanks to M. M. Backus whose many corrections, comments, and ideas made this review somewhat more acceptable. F. Hilterman's unpublished course

notes were an invaluable reference. Thanks to ARCO Oil and Gas Co. for permission to publish this paper.

REFERENCES

Aki, K., and Richards, P. G., 1980, Quantitative seismology: Theory and methods: W. H. Freeman and Co.

Angerer, R. H., and Richgels, H. J., 1990, Reservoir states and elastic parameters: Factors which affect reflection AVO: 60th Ann. Internat. Mtg., Soc. Expl. Geophys., Expanded Abstracts, 1537–1538.

Anstey, N. A., 1977, Seismic interpretation: The physical aspects: International Human Resources Development Corporation.

Assous, F., and Richard, V., 1989, Full elastic inversion of multioffset marine data on a stratified medium: 59th Ann. Internat. Mtg., Soc. Expl. Geophys., Expanded Abstracts, 959–962.

Backus, M. M., 1987, Amplitude versus offset: A review: 57th Ann. Internat. Mtg., Soc. Expl. Geophys., Expanded Abstracts, 359–364.

Ball, V., 1988, Thin bed tuning analysis using AVO stratigraphy methods: 58th Ann. Internat. Mtg., Soc. Expl. Geophys., Expanded Abstracts, 1213–1216.

Balogh, D., and Snyder, G., 1986, Examples of a new approach to offset amplitude analysis: 56th Ann. Internat. Mtg., Expanded Abstracts, 350–351.

Berkhout, A. J., and Wapenaar, C. P. A., 1988, Delft philosophy on inversion of elastic data: 58th Ann. Internat. Mtg., Soc. Expl. Geophys., Expanded Abstracts, 831–833.

Bernitsas, N., 1990, Curvature effect of a reflecting surface for arbitrary offset and azimuth., 60th Ann. Internat. Mtg., Soc. Expl. Geophys., Expanded Abstracts, 1053–1055.

Bortfeld, R., 1961, Approximation to the reflection and transmission coefficients of plane longitudinal and transverse waves: Geophys. Prosp., **9**, 485–503.

Burnett, R. C., 1989, Seismic amplitude anomalies and AVO analysis at Mestena Grande field: 59th Ann. Internat. Mtg., Soc. Expl. Geophys., Expanded Abstracts, 690–694.

Burnett, R. C., 1990, Seismic amplitude anomalies and AVO analysis at Mestena Grande field: Geophysics, **55**, 1015–1025.

Carazzone, J. J., and Srnka, L. J., 1989, Elastic inversion of Gulf of Mexico data: 59th Ann. Internat. Mtg., Soc. Expl. Geophys., Expanded Abstracts, 956–958.

Castagna, J. P., Batzle, M. L., and Eastwood, R. L., 1985, Relationship between compressional and shear-wave velocities in clastic silicate rocks: Geophysics, **50**, 551–570.

Castagna, J. P., Batzle, M. L., and Kan, T. K., 1993, Rock physics: the link between rock properties and AVO response *in* Castagna, J. P., and Backus, M. M., Eds., Offset-dependent reflectivity—Theory and practice of AVO analysis, Soc. Expl. Geophys., 135–171.

Cerveny, V., and Ravindra, R., 1971, Theory of seismic head waves: Univ. of Toronto Press.

Chacko, S., 1989, Porosity identification using amplitude variations with offset: Examples from South Sumatra: Geophysics, **54**, 942–951.

Chiburis, E. F., 1984, Analysis of amplitude versus offset to detect gas-oil contacts in the Arabia Gulf: 54th Ann. Internat. Mtg., Soc. Expl. Geophys., Expanded Abstracts, 669–670.

Chiburis, E. F., 1987, Studies of amplitude versus offset in Saudi Arabia: 57th Ann. Internat. Mtg., Soc. Expl. Geophys., Expanded Abstracts, 614–616.

Chiburis, E. F., and Al-Faraj, 1987, Depthing shallow reflectors using postcritical P-wave reflection amplitudes: 57th Ann. Internat. Mtg., Soc. Expl. Geophys., Expanded Abstracts, 631–633.

Coruh, C., and Demirbag, E., 1989, Zoeppritz amplitude correction: Is it needed?: 59th Ann. Internat. Mtg., Soc. Expl. Geophys., Expanded Abstracts, 1160–1163.

Danbom, S. H., and Domenico, S. N., 1986, Shear-wave exploration: Geophysical Development Series, Volume 1, Soc. Expl. Geophys.

de Bruin, C. G. M., Wapenaar, C. P. A., and Berkhout, A. J., 1988, Angle-dependent reflectivity by shot record migration: 58th Ann. Internat. Mtg., Soc. Expl. Geophys., Expanded Abstracts, 1093–1096.

de Bruin, C. G. M., Wapenaar, C. P. A., and Berkhout, A. J., 1990, Imaging for angle-dependent reflectivity in the presence of dip: 60th Ann. Internat. Mtg., Soc. Expl. Geophys., Expanded Abstracts, 1503–1506.

de Haas, J. C., and Berkhout, A. J., 1988, On the information content of *P-P*, *P-SV*, *SV-SV*, and *SV-P* Reflections: 58th Ann. Internat. Mtg., Soc. Expl. Geophys., Expanded Abstracts, 1190–1194.

de Haas, J. C., and Berkhout, A. J., 1989, Practical approach to nonlinear inversion of amplitude versus offset information: 59th Ann. Internat. Mtg., Soc. Expl. Geophys., Expanded Abstracts, 839–842.

Denham, L. R., Palmeira, R. A. R., and Farrell, R. C., 1985, The zero-offset stack: 55th Ann. Internat. Mtg., Soc. Expl. Geophys., Expanded Abstracts, 624–625.

Dey-Sarkar, S. K., Dutta, N. C., Weglein, A. B., Backus, M. M., and Hilterman, F., 1988, Amplitude versus offset workshop: 58th Ann. Internat. Mtg., Soc. Expl. Geophys., Expanded Abstracts, 1353–1359.

Dey-Sarkar, S. K., and James, C. F., 1986, Prestack analysis: relevance of petrophysical properties: 56th Ann. Internat. Mtg., Soc. Expl. Geophys., Expanded Abstracts, 337–339.

Domenico, S. N., 1976, Effect of brine-gas mixture on velocity in an unconsolidated sand reservoir: Geophysics, **41**, 882–894.

Du, X., and Spencer, T. W., 1990, Quantitative analysis of amplitude versus offset: 60th Ann. Internat. Mtg., Soc. Expl. Geophys., Expanded Abstracts, 1459–1462.

Duren, R. E., 1990, Seismic range equation: 60th Ann. Internat. Mtg., Soc. Expl. Geophys., Expanded Abstracts, 1495–1498.

Duren, R. E., 1991, Seismic range equation: Geophysics, **56**, 1015–1026.

Duren, R. E., 1992, Range-equation weights for AVO: Geophysics, **57**, 1203–1208.

Dutta, N. C., and Ode, H., 1981, Biot loss mechanism and its importance in seismology: A review: 51st Ann. Internat. Mtg., Soc. Expl. Geophys., Abstracts, 103–104.

Dutta, N. C., and Ode, H., 1983, Seismic reflections from a gas-water contact: Geophysics, **48**, 148–162.

Fouquet, D. F., 1990, Principles of AVO processing: 60th Ann. Internat. Mtg., Soc. Expl. Geophys., Expanded Abstracts, 1486.

Frasier, C. W., 1988, AVO: usage/misusage: 58th Ann. Internat. Mtg., Soc. Expl. Geophys., Expanded Abstracts, 1356.

Fuller, B. N., Iverson, W. P., and Smithson, S. B., 1989, AVO for thin sand bed detection: 59th Ann. Internat. Mtg., Soc. Expl. Geophys., Expanded Abstracts, 826–828.

Gabay, S. H., 1990, Integrated lithologic interpretation of normal and nonnormal-incidence reflection character: 60th Ann. Internat. Mtg., Soc. Expl. Geophys., Expanded Abstracts, 1519–1522.

Garotta, R., 1988, Amplitude-versus-offset measurements involving converted waves: 58th Ann. Internat. Mtg., Soc. Expl. Geophys., Expanded Abstracts, 1357.

Garotta, R., and Granger, P. Y., 1987, Comparison of responses of compressional and converted waves on a gas sand: 57th Ann. Internat. Mtg., Soc. Expl. Geophys., Expanded Abstracts, 627–630.
Gassaway, G. S., 1984, Effects of shallow reflectors on amplitude versus offset (seismic lithology) analysis: 54th Ann. Internat. Mtg., Soc. Expl. Geophys., Expanded Abstracts, 665–669.
Gassmann, F., 1951, Elastic waves through a packing of spheres: Geophysics, **16**, 673–685.
Gelfand, V., Ng, P., Nguyen, H., and Larner, K., 1986, Seismic lithologic modeling of amplitude versus offset data: 56th Ann. Internat. Mtg., Soc. Expl. Geophys., Expanded Abstracts, 334–337.
Greenberg, M. L., and Castagna, J. P., 1992, Shear-wave velocity estimation in porous rocks: Theoretical formulation, preliminary verification and applications: Geophys. Prosp., **40**, 195–209.
Gregory, A. R., 1976, Fluid saturation effects on dynamic elastic properties of sedimentary rocks: Geophysics, **41**, 895–921.
Hales, A. L., and Roberts, J. L., 1974, The Zoeppritz amplitude equations: more errors: Bull., Seis. Soc. Am., **64**, 285
Hampson, D., and Russell, B., 1990, AVO inversion: theory and practice: 60th Ann. Internat. Mtg., Soc. Expl. Geophys., Expanded Abstracts, 1456–1458.
Herman, G. C., and Bionk, B., 1990, Influence of small-scale interface roughness in the estimation of lithologic parameters from reflection coefficients: 60th Ann. Internat. Mtg., Soc. Expl. Geophys., Expanded Abstracts, 1475–1478.
Hilterman, F., 1975, Amplitudes of seismic waves—a quick look., Geophysics, **40**, 745–762.
Hilterman, F., 1989, Is AVO the seismic signature of rock properties?: 59th Ann. Internat. Mtg., Soc. Expl. Geophys., Expanded Abstracts, 559.
Hilterman, F., 1990, Is AVO the seismic signature of lithology? A case history of Ship Shoal—South Addition, Leading Edge, 9, no. 6, 15–22.
Hindlet, F. J. F., and McDonald, J. A., 1986, Thin layer analysis using offset/amplitude data: 56th Ann. Internat. Mtg., Soc. Expl. Geophys., Expanded Abstracts, 346–349.
Hoopes, R., and Aber, W. M., 1989, Integrated multianalysis procedure that qualifies DHIs: A case history of the Louisiana Hackberry Trend: 59th Ann. Internat. Mtg., Soc. Expl. Geophys., Expanded Abstracts, 843–847.
Huston, D. C., and Backus, M. M., 1986, Interpretation of seismic signal and noise through line intersection analysis: 56th Ann. Internat. Mtg., Soc. Expl. Geophys., Expanded Abstracts, 501–503.
Hwang, L. F., and Lellis, P. J., 1988, Bright spots related to high GOR oil reservoir in Green Canyon: 58th Ann. Internat. Mtg., Soc. Expl. Geophys., Expanded Abstracts, 761–763.
Ikelle, L. T., Diet, J. P., and Tarantola, A., 1986, Linearized inversion of multioffset seismic reflection data in ω-k domain with depth-dependent reference medium: 56th Ann. Internat. Mtg., Soc. Expl. Geophys., Expanded Abstracts, 530–533.
Ito, H., DeVilbiss, J., and Nur, A., 1979, Compressional and shear waves in saturated rock during water-steam transition: J. Geophys. Res., **84**, 4731–4735.
Johnson, W. E., 1988, Amplitude versus offset for sandstones in shales and carbonates., 58th Ann. Internat. Mtg., Soc. Expl. Geophys., Expanded Abstracts, 593–595.
Kelamis, P. G., Chiburis, E. F., and Shabryar, S., 1990, Radon multiple elimination, a practical methodology for land data: 60th Ann. Internat. Mtg., Soc. Expl. Geophys., Expanded Abstracts, 1611–1613.
Knott, C. G., 1899, Reflexion and refraction of elastic waves with seismological applications: Phil. Mag., **48**, 64–97.
Koefoed, O., 1955, On the effect of Poisson's ratios of rock strata on the reflection coefficients of plane waves: Geophys. Prosp., **3**, 381–387.
Kolb, O., Chapel, F., and Picart, I., 1989, Lithologic inversion: a reflectivity versus angle (RVA) approach: 59th Ann. Internat. Mtg., Soc. Expl. Geophys., Expanded Abstracts, 695–699.
Krail, P. M., and Brysk, H., 1983, Reflection of spherical seismic waves in elastic layered media: Geophysics, **48**, 655–664.
Long, A., and Richgels, J., 1985, A practical application of amplitude versus offset effects: 55th Ann. Internat. Mtg., Soc. Expl. Geophys., Expanded Abstracts, 594–598.
Lortzer, G. J. M., and Berkhout, A. J., 1989, Linear AVO inversion of multicomponent seismic data: 59th Ann. Internat. Mtg., Soc. Expl. Geophys., Expanded Abstracts, 967–972.
Lortzer, G. J. M., de Haas, J. C., and Berkhout, A. J., 1988, Evaluation of weighted stacking techniques for AVO inversion: 58th Ann. Internat. Mtg., Soc. Expl. Geophys., Expanded Abstracts, 1204–1208.
Luh, P. C., 1988, Wavelet dispersion and bright spot detection: 58th Ann. Internat. Mtg., Soc. Expl. Geophys., Expanded Abstracts, 1217–1220.
MacLeod, M. K., and Martin, H. L., 1988, Amplitude changes due to bed curvature: 58th Ann. Internat. Mtg., Soc. Expl. Geophys., Expanded Abstracts, 1209–1212.
Makris, J., and Thiessin, J., 1984, Wide-angle reflections: a tool to penetrate horizons with high acoustic impedance contrasts: 54th Ann. Internat. Mtg., Soc. Expl. Geophys., Expanded Abstracts, 672–674.
Mazzotti, A., 1984, Prestack analysis of seismic amplitude anomalies: 54th Ann. Internat. Mtg., Soc. Expl. Geophys., Expanded Abstracts, 659–661.
Mazzotti, A., 1990, Prestack amplitude analysis methodology and application to seismic bright spots in the Po Valley, Italy: Geophysics, **55**, 157–166.
Miles, D. R., and Gassaway, G. S., 1989, Three-component AVO analysis: 59th Ann. Internat. Mtg., Soc. Expl. Geophys., Expanded Abstracts, 706–708.
Mora, P., 1984, Inversion of CMP gathers for P- and S-velocity: 54th Ann. Internat. Mtg., Soc. Expl. Geophys., Expanded Abstracts, 730–733.
Mora, P., 1986, Nonlinear elastic inversion of multioffset seismic data: 56th Ann. Internat. Mtg., Soc. Expl. Geophys., Expanded Abstracts, 533–537.
Mora, P., 1987a, Elastic inversion of multi-offset seismic amplitude data for *P*-wave velocity, *S*-wave velocity, and density *in* Danbom, S. H., and Domenico, S. N., Editors, Shear-wave Exploration, Geophysical Developments No. 1, 199–213, Soc. Expl. Geophys.
Mora, P., 1987b, Nonlinear two-dimensional elastic inversion of multioffset seismic data: Geophysics, **52**, 1211–1228.
Mora, P., 1987c, Nonlinear elastic inversion of real data: 57th Ann. Internat. Mtg., Soc. Expl. Geophys., Expanded Abstracts, 430–432.
Mora, P., 1988, Elastic wave-field inversion of reflection and transmission data: Geophysics, **53**, 750–759.
Morley, L., 1984, Invertibility of elastic layered earth parameters from precritical *P*-wave reflection amplitudes: 54th Ann. Internat. Mtg., Soc. Expl. Geophys., Expanded Abstracts, 641–643.
Murphy, W. F., 1982, Effects of microstructure and pore fluids on acoustic properties of granular sedimentary materials: Ph.D. dissertation, Stanford Univ.

Muskat, M., and Meres, M. W., 1940, Reflection and transmission coefficients for plane waves in elastic media: Geophysics, **5**, 115–148.
Nelson, V., 1989, Display techniques for AVO analysis: 59th Ann. Internat. Mtg., Soc. Expl. Geophys., Expanded Abstracts, 447–448.
Newman, P., 1973, Divergence effects in a layered earth: Geophysics, **38**, 481–488.
Onstott, G. E., 1984, Processing and display of offset dependent reflectivity in reflection seismograms: M.Sc. thesis, Univ. of Texas at Austin.
Onstott, G. E., Backus, M. M., Wilson, C. R., and Phillips, J. D., 1984, Color display of offset dependent reflectivity in seismic data: 54th Ann. Internat. Mtg., Soc. Expl. Geophys. Expanded Abstracts, 674–675.
Ostrander, W. J., 1982, Method for interpretation of seismic records to yield indication of gaseous hydrocarbons: United States Patent No. 4,316,268.
Ostrander, W. J., 1984, Plane-wave reflection coefficients for gas sands at nonnormal angles of incidence: Geophysics, **49**, 1637–1648.
Pan, G. S., Young, C. Y., and Castagna, J. P., 1990, Sensitivity and resolution of an integrated target-oriented prestack elastic inversion: 60th Annual Internat. Mtg., Soc. Expl. Geophys., Expanded Abstracts, 1173–1176.
Parson, R., 1986, Estimating reservoir mechanical properties using constant offset images of reflection coefficients and incident angles: 56th Ann. Internat. Mtg., Expanded Abstracts, 617–620.
Payne, M. A., 1991, Shear-wave logging to enhance seismic modeling: Geophysics, **56**, 2129–2138.
Pigott, J. D., Shrestha, R. K., and Warwick, R. A., 1990, Direct determination of carbonate reservoir porosity and pressure from AVO inversion: 60th Ann. Internat. Mtg., Soc. Expl. Geophys., Expanded Abstracts, 1533–1536.
Poley, D. F., Lawton, D. C., and Blasco, S. M., 1989, Amplitude-offset relationships over shallow velocity inversions: Geophysics, **54**, 1114–1122.
Rafipour, B., 1987, Seismic response for reservoir fluid evaluation: 57th Ann. Internat. Mtg., Soc. Expl. Geophys., Expanded Abstracts, 377–380.
Ramirez, L. C., 1990, AVO statistical analysis: a useful tool for interbedded salt body detection: 60th Ann. Internat. Mtg., Soc. Expl. Geophys., Expanded Abstracts, 1483–1485.
Rendleman, C. A., and Levin, F. K., 1988, Reflection maxima for reflections from single interfaces: Geophysics, **53**, 271–275.
Resnick, J. R., Ng, P., and Larner, K., 1987, Amplitude versus offset analysis in the presence of dip: 57th Ann. Internat. Mtg., Soc. Expl. Geophys., Expanded Abstracts, 617–620.
Resnick, J. R., 1988, Seismic data processing for amplitude-versus-offset analysis: 58th Ann. Internat. Mtg., Soc. Expl. Geophys., Expanded Abstracts, 1354.
Richards, P. G., and Frasier, C. W., 1976, Scattering of elastic waves from depth-dependent inhomogeneities: Geophysics, **41**, 441–458.
Richards, T. C., 1961, Motion of the ground on arrival of reflected longitudinal and transverse waves at wide-angle reflection distances: Geophysics, **26**, 277–297.
Rosa, A. L. R., 1976, Extraction of elastic parameters using seismic reflection amplitude with offset variation: M.A. Thesis, Univ. of Houston.
Rutherford, S. R., and Williams, R. H., 1989, Amplitude-versus-offset variations in gas sands: Geophysics, **54**, 680–688.
Samec, P., Blangy, J. P., and Nur, A., 1990, Effect of viscoelasticity and anisotropy on amplitude-versus-offset interpretation: 60th Ann. Internat. Mtg., Soc. Expl. Geophys., Expanded Abstracts, 1479–1482.
Sengupta, M. K., and Rendleman, C. A., 1989, Case study: the importance of gas leakage in interpreting amplitude-versus-offset (AVO) analysis: 59th Ann. Internat. Mtg., Soc. Expl. Geophys., Expanded Abstracts, 848–850, and Geophys., **56**, 1886–1895.
Sherwood, J., Kan, T. K., and Crampin, S., 1983, Synthetic seismograms in a solid layered earth: 53rd Ann. Internat. Mtg., Soc. Expl. Geophys., Expanded Abstracts, 636
Shuey, R. T., Banik, N. C., and Lerche, I., 1984, Amplitude from curved reflectors: 54th Ann. Internat. Mtg., Soc. Expl. Geophys., Expanded Abstracts, 664–665.
Shuey, R. T., 1985, A simplification of the Zoeppritz equations: Geophysics, **50**, 609–614.
Smith, G. C., and Gidlow, P. M., 1987, Weighted stacking for rock property estimation and detection of gas: Geophys. Prosp., **35**, 993–1014.
Snyder, A. G., Kelsey, D. J., and Wrolstad, K. H., 1989, Direct detection using AVO, Central Graben, North Sea: 59th Ann. Internat. Mtg., Soc. Expl. Geophys., Expanded Abstracts, 700–701.
Soroka, W. L., Fitch, T. J., Van Sickle, K. H., and North, P. D., 1990, Three-dimensional AVO analysis: 60th Ann. Internat. Mtg., Soc. Expl. Geophys., Expanded Abstracts, 1530–1532.
Spratt, S., 1987, Effect of normal moveout errors on amplitude versus offset-derived shear reflectivity: 57th Ann. Internat. Mtg., Soc. Expl. Geophys., Expanded Abstracts, 634–637.
Spratt, R. S., Goins, N. R., and Fitch, T. J., 1993, Pseudo-shear: The analysis of AVO *in* Castagna, J. P., and Backus, M. M., Eds., Offset-dependent reflectivity, Soc. Expl. Geophys. 37–56.
Stoll, R. D., and Kan, T. K., 1981, Reflection of acoustic waves at a water-sediment interface: J. Acoust. Soc. Am., **70**, 149–156.
Stolt, R. H., and Weglein, A. B., 1985, Migration and inversion of seismic data: Geophysics, **50**, 2458, 2472.
Strudley, A., 1990, Amplitude versus offset: Methodology and application to pore fill prediction in the Danish Central Graben: 60th Ann. Internat. Mtg., Soc. Expl. Geophys., Expanded Abstracts, 1523–1525.
Sumner, J. R., 1988, Amplitude versus offset: The transfer of a complex technology: 58th Ann. Internat. Mtg., Soc. Expl. Geophys., Expanded Abstracts, 1358–1359.
Swan, H. W., 1988, Amplitude versus offset analysis in a finely layered media: 58th Ann. Internat. Mtg., Soc. Expl. Geophys., Expanded Abstracts, 1195–1198.
Tarantola, A., Crase, E., Jervis, M., Konen, Z., Lindgren, J., Mosegaard, K., and Noble, M., 1990, Nonlinear inversion of seismograms: State of the art: 60th Ann. Internat. Mtg., Soc. Expl. Geophys., Expanded Abstracts, 1193–1198.
Tarantola, A., Beydoun, W., Cao, D., Crase, E., Koren, Z., Mendes, M., Mora, P., Mosegaard, K., Noble, M., Singh, S., and Trezeguet, D., 1989, Present know-how and difficulties in elastic nonlinear inversion of seismograms: 59th Ann. Internat. Mtg., Soc. Expl. Geophys., Expanded Abstracts, 980–982.
Todd, C. P., and Backus, M. M., 1985, Offset-dependent-reflectivity in a structural context: 55th Ann. Internat. Mtg., Soc. Expl. Geophys., Expanded Abstracts, 586–589.
Todd, C. P., 1986, Isolation, display and interpretation of offset dependent phenomena in seismic reflection data using offset to depth (ODR) range partial stacking., M.Sc. thesis, Univ. Texas Austin.
Treadgold, G. E., Dey-Sarkar, S. K., Smith, S. W., and Swan, H. W., 1990a, Amplitude versus offset and thin

beds: 60th Ann. Internat. Mtg., Soc. Expl. Geophys., Expanded Abstracts, 1463–1466.
Treadgold, G. E., Ritchie, K., and Dey-Sarkar, S. K., 1990b, AVO: An example of processing pitfalls: 60th Ann. Internat. Mtg., Soc. Expl. Geophys., Expanded Abstracts, 1487–1490.
Tsingas, C., and Kanasewich, E. R., 1991, Seismic reflection amplitude versus angle variations over a thermally enhanced oil recovery site: Geophysics, **56**, 292–301.
Wang, D., Beylkin, G., Burridge, R., and Chang, H. W., 1990, GRT inversion for elastic parameters using *PP*, *PS*, *SP*, and *SS* seismic data: 60th Ann. Internat. Mtg., Soc. Expl. Geophys., Expanded Abstracts, 1199–1202.
Wapenaar, C. P. A., Verschuur, D. J., and Herrmann, P., 1990, Amplitude preprocessing of 2-D seismic data: 60th Ann. Internat. Mtg., Soc. Expl. Geophys., Expanded Abstracts, 1491–1494.
Waters, K. H., 1981, Reflection Seismology: A tool for energy resource exploration: John Wiley & Sons, Inc.
Widess, M. B., 1973, How thin is a thin bed?: Geophysics, **38**, 1176–1180.
Wiggins, R., Kenny, G. S., and McClure, C. D., 1983, A method for determining and displaying the shear-velocity reflectivities of a geologic formation: European Patent Application 0113944.
Wright, J., 1984, The effects of anisotropy on reflectivity-offset: 54th Ann. Internat. Mtg., Soc. Expl. Geophys., Expanded Abstracts, 670–672.
Wrolstad, K. H., 1986, Offset-dependent amplitude analysis by visco-elastic lithological modeling: 56th Ann. Internat. Mtg., Soc. Expl. Geophys., Expanded Abstracts, 341–346.
Wrolstad, K. H., 1988, AVO representations: 58th Ann. Internat. Mtg., Soc. Expl. Geophys., Expanded Abstracts, 1355.
Xu, Y., and McDonald, J. A., 1988, Effects of velocity variation on AVO and AVA calculations: 58th Ann. Internat. Mtg., Soc. Expl. Geophys., Expanded Abstracts, 1221–1223.
Young, G. B., and Braile, L. W., 1976, A computer program for the application of Zoeppritz' amplitude equations: Seis. Soc. Am. Bull., **52**, 923–956.
Yu, G., 1985(a), Offset amplitude variation and controlled amplitude processing: 55th Ann. Internat. Mtg., Soc. Expl. Geophys., Expanded Abstracts, 591–594.
Zilik, R. P., 1989, Seismic bright spots: detecting Yegua channel sands using velocity inversion: 59th Ann. Internat. Mtg., Soc. Expl. Geophys., Expanded Abstracts, 829–831.
Zimmerman, C. J., and Fahmy, B. A., 1990, An effective new method of amplitude-versus-offset analysis for marine data: 60th Ann. Internat. Mtg., Soc. Expl. Geophys., Expanded Abstracts, 1499–1502.
Zoeppritz, K., 1919, Erdbebenwellen VIIIB, On the reflection and propagation of seismic waves: Gottinger Nachrichten, I, 66–84.

REFERENCES FOR GENERAL READING

Backus, M. M., and Chen, R. L., 1975, Flat-spot exploration: Geophys. Props., **23**, 533–577.
Backus, M. M., Garcia, A. I., and Huston, D. C., 1987, On deconvolution and inversion in a one-dimensional earth: Proceedings SEG-EAEG workshop on deconvolution and inversion, Rome.
Backus, M. M., and Goins, N. R., 1983, Research workshop 2—the change in reflectivity with offset: 53rd Ann. Internat. Mtg., Soc. Expl. Geophys., Expanded Abstracts, 636.
Backus, M. M., Nepomuceno, F., and Cao, J., 1982, The reflection seismogram in a solid layered earth: 52nd Ann. Internat. Mtg., Soc. Expl. Geophys., Expanded Abstracts, 218–220.
Backus, M. M., Nepomuceno, F., and Cao, J., 1983, Reflection seismogram in a solid layered earth: Abstract, Bull. Am. Assn. Petr. Geol., 416–417.
Ball, V., 1987, Depth inversion of impedance and Poisson's Ratio using the Insight interactive modeling system: 57th Ann. Internat. Mtg., Soc. Expl. Geophys., Expanded Abstracts, 624–626.
Carrion, P. M., and Foster, D. J., 1985, Inversion of seismic data using precritical reflection and refraction data: Geophysics, **50**, 759–765.
Clark, V. A., 1992, The effect of oil under in-situ conditions on the seismic properties of rocks: Geophysics, **57**, 894–901.
Cunha, C. A., Jr., 1990, Snell-beam transform: retrieving the angle-dependent reflectivity: 60th Ann. Internat. Mtg., Soc. Expl. Geophys., Expanded Abstracts, 1507–1510.
Daggett, P. H., Young, C. Y., and Kan, T. K., 1983, Comparison of prestack acoustic and elastic synthetic seismograms: 53rd Ann. Internat. Mtg., Soc. Expl. Geophys., Expanded Abstracts, 457–458.
de Beukelaar, P., and Richard, V., 1990, Source estimation and lateral sensitivity of nonlinear inversion for multioffset seismic surface data: 60th Ann. Internat. Mtg., Soc. Expl. Geophys., Expanded Abstracts, 1161–1164.
de Haas, J. C., and Berkhout, A. J., 1990, Local inversion of *PP*, *PS*, *SP*, and *SS* reflections: 60th Ann. Internat. Mtg., Soc. Expl. Geophys., Expanded Abstracts, 1189–1192.
Demirbag, E., and Coruh, C., 1988, Inversion of Zoeppritz equations and their approximations: 58th Ann. Internat. Mtg., Soc. Expl. Geophys., Expanded Abstracts, 1199–1203.
Demirbag, E., and Coruh, C., 1989, Inversion of multilayer amplitude versus offset data: 59th Ann. Internat. Mtg., Soc. Expl. Geophys., Expanded Abstracts, 709–712.
Dey-Sarkar, S. K., 1986, Prestack analysis: Data processing: 56th Ann. Internat. Mtg., Soc. Expl. Geophys., Expanded Abstracts, 339–341.
Domenico, S. N., 1974, Effect of water saturation on seismic reflectivity of sand reservoirs encased in shale: Geophysics, **39**, 759–769.
Foster, D. J., and Mosher, C. C., 1992, Suppression of multiple reflections using the Radon transform: Geophysics, **57**, 386–395.
Fulton, T. K., and Darr, K. M., 1984, Offset panel: Geophysics, **49**, 1140–1152.
Garcia, A., and Backus, M. M., 1985, Thin layer resonse catalog, 55th Ann. Internat. Mtg., Soc. Expl. Geophys., Expanded Abstracts, 588–590.
Gardner, G. H. F., Gardner, L. W., and Gregory, A. R., 1974, Formation velocity and density—the diagnostic basis for stratigraphic traps: Geophysics, **39**, 770–780.
Gassaway, G. S., 1983, Comparison and application of synthetic plane wave front CDP seismograms and observed CDP gathers from the Sacramento Valley and Denver-Julesburg Basin: 53rd Ann. Internat. Mtg., Soc. Expl. Geophys., Expanded Abstracts, 638.
Gassaway, G. S., Brown, R. A., and Bennett, L. E., 1986, Pitfalls in seismic amplitude-versus-offset analysis: case histories: 56th Ann. Internat. Mtg., Soc. Expl. Geophys., Expanded Abstracts, 332–334.
Gassaway, G. S., and Richgels, H. J., 1983, SAMPLE: Seismic amplitude measurement from primary lithology estimation: 53rd Ann. Internat. Mtg., Soc. Expl. Geophys., Expanded Abstracts, 610–613.
Gassaway, G. S., and Richgels, H. J., 1984, Seismic amplitude measurement for primary lithology estimation (SAM-

PLE): Case histories from Tertiary western basins: Offshore Tech. Conf. 4784.
Han, D. H., Nur, A., and Morgan, D., 1986, Effects of porosity and clay content on wave velocities in sandstones: Geophysics, **51**, 2093–2107.
Hindlet, F., Chapel, F., and Picart, I., 1990, Increasing the sensitivity of AVO data for reservoir characterization: 60th Ann. Internat. Mtg., Soc. Expl. Geophys., Expanded Abstracts, 1457–1470.
Huston, D. C., and Backus, M. M., 1989, Offset-dependent mis-tie analysis at seismic line intersections: Geophysics, **54**, 962–972.
Jervis, M., 1990, Simultaneous recovery of the source wavelet and seismic impedances by nonlinear elastic inversion: 60th Ann. Internat. Mtg., Soc. Expl. Geophys., Expanded Abstracts, 1158–1160.
Johnson, W. E., 1990, Amplitude-versus-offset analysis for sandstones encased in carbonates and shales., 60th Ann. Internat. Mtg., Soc. Expl. Geophys., Expanded Abstracts, 1526–1529.
Kanasewich, E. R., and Tsingas, C., 1990, Amplitude and ratio for partial angle (ARPA): a new method for imaging amplitude-versus-offset seismic reflection data: 60th Ann. Internat. Mtg., Soc. Expl. Geophys., Expanded Abstracts, 1516–1518.
Kind, R., 1976, Computation of reflection coefficients for layered media, J. of Geophysics, **42**, 191–200.
Koefoed, O., 1962, Reflection and transmission coefficients for plane longitudinal and incident waves: Geophys. Prosp., **10**, 304–351.
Kolb, P., and Canadas, G., 1986, Least-squares inversion of prestack data: simultaneous identification of density and velocity of stratified media: 56th Ann. Internat. Mtg., Soc. Expl. Geophys., Expanded Abstracts, 604–607.
Kolb, P., Collino, F., and Lailly, P., 1986, Prestack inversion of 1-D medium: Proc. Inst. Electr. Electron. Eng., Special Issue, Seismic Inverse Problems.
Levin, F. K., 1986, When reflection coefficients are zero: Geophysics, **51**, 736–741.
Lin, T. L., 1989, AVO modeling by domain classification: 59th Ann. Internat. Mtg., Soc. Expl. Geophys., Expanded Abstracts, 702–705.
Lortzer, G. J. M., and Berkhout, A. J., 1990, Influence of lithology and data quality on lithologic inversion results: 60th Ann. Internat. Mtg., Soc. Expl. Geophys., Expanded Abstracts, 1185–1188.
Luh, P. C., 1992, True-amplitude signal recovery: The Leading Edge, **11**, no. 2, 13–24.
Martinez, R. D., and McMechan, G. A., 1988, Multiparameter inversion for viscoelastic media: 58th Ann. Internat. Mtg., Soc. Expl. Geophys., Expanded Abstracts, 853–855.
Masuda, R. M., 1990, Patterm recognition of AVO and amplitude anomalies in exploration seismology: 60th Ann. Internat. Mtg., Soc. Expl. Geophys., Expanded Abstracts, 1539–1540.
Mazzotti, A., 1988, Methodology of prestack amplitude analysis and its application to seismic bright spots in the Po Valley, Italy: 58th Ann. Internat. Mtg., Soc. Expl. Geophys., Expanded Abstracts, 756–760.
McCarthy, C. J., 1984, Seismic prediction of pore fluid and gas thickness: 54th Ann. Internat. Mtg., Soc. Expl. Geophys., Expanded Abstracts, 326–328.
McCauley, A. D., 1984, Importance of shear in plane layer point source modeling for prestack inversion: 54th Ann. Internat. Mtg., Soc. Expl. Geophys., Expanded Abstracts, 541–544.
McCauley, A. D., 1985, Prestack inversion with plane-layer point source modeling, Geophys., **50**, 77–89.
McCauley, A. D., 1986, Plane-layer point-source prestack inversion of marine data with unknown initial profile: 56th Ann. Internat. Mtg., Soc. Expl. Geophys., Expanded Abstracts, 537–539.
Miles, D. R., Gassaway, G. S., Bennett, L. E., and Brown, R. A., 1988, Detecting hydrocarbons in reefs using AVO analysis: A case history from Alberta, Canada: 58th Ann. Internat. Mtg., Soc. Expl. Geophys., Expanded Abstracts, 753–755.
Muskat, M., and Meres, M. W., 1940, The seismic wave energy reflected from various types of stratified horizons: Geophysics, **5**, 149–155.
Neidell, N. S., 1985, Geophysical determination of lithology, using shear waves and amplitudes with offsets—a progress update: Continuing Education Course Note Series #29, Am. Assn. Petr. Geol.
Neidell, N. S., 1985, A progress report on use of shear waves and amplitude with offset in seismic exploration: Leading Edge, **4**, 10, 92–93.
Neidell, N. S., 1986, Amplitude variation with offset: Leading Edge, **5**, 1, 47–51.
Neidell, N. S., 1986, Research elements in amplitude variation with offset: Leading Edge, **5**, 4, 42–44.
Normington, E. J., 1990, Seismic model studies of the overburden bedrock reflection: *P*-wave and *S*-wave: 60th Ann. Internat. Mtg., Soc. Expl. Geophys., Expanded Abstracts, 376–379.
Ostrander, W. J., 1982b, Plane-wave reflection coefficients for gas sands at nonnormal angles of incidence: 52nd Ann. Internat. Mtg., Soc. Expl. Geophys., Expanded Abstracts, 216–220.
Ostrander, W. J., and Gassaway, G., 1983, The use of offset dependent reflectivity in exploration: 53rd Ann. Internat. Mtg., Soc. Expl. Geophys., Expanded Abstracts, 637.
Pan, G. S., and Phinney, R. A., 1986, Full waveform inversion of p-τ seismogram: 56th Ann. Internat. Mtg., Soc. Expl. Geophys., Expanded Abstracts, 614–617.
Pan, N. D., and Gardner, G. H. F., 1986, The p,q algorithm for seismic data analysis: 56th Ann. Internat. Mtg., Soc. Expl. Geophys., Expanded Abstracts, 413–417.
Pigott, J. D., 1989, Young's modulus from AVO inversion: 59th Ann. Internat. Mtg., Soc. Expl. Geophys., Expanded Abstracts, 832–835.
Pullan, S. E., and Hunter, J. A., 1985, Seismic model studies of the overburden bedrock reflection: Geophysics, **50**, 1684–1688.
Rafipour, B., and Herrin, E., 1986, Phase offset indicator (POI): A study of phase shift versus offset and fluid content: Geophysics, **51**, 679–688.
Regueiro, J., 1989, Gas sand reservoirs: low versus high porosity in their seismic perspective: 59th Ann. Internat. Mtg., Soc. Expl. Geophys., Expanded Abstracts, 822–825.
Richter, C. F., 1958, Elementary seismology: San Francisco, Freeman and Co., 670–672.
Ross, C. P., 1992, Incomplete AVO near salt structures: Geophysics, **57**, 543–553.
Samec, P., and Blangy, J. P., 1992, Viscoelastic attenuation, anisotropy, and AVO: Geophysics, **57**, 441–450.
Schneider, W. A., and Goins, N., 1983, General implications of offset-dependent reflectivity and converted waves: 53rd Ann. Internat. Mtg., Soc. Expl. Geophys., Expanded Abstracts, 638.
Sengupta, M. K., 1987, Sensitivity analysis of amplitude versus offset (AVO) method: 57th Ann. Internat. Mtg., Soc. Expl. Geophys., Expanded Abstracts, 621–623.
Shang, Z., McDonald, J. A., and Gardner, G. H. F., 1989, Extraction of amplitude versus incident angle information in the presence of structure: 59th Ann. Internat. Mtg., Soc. Expl. Geophys., Expanded Abstracts, 713–715.
Shang, Z., McDonald, J. A., and Gardner, G. H. F., 1990,

Automated extraction of amplitude versus incident angle information in the presence of structure: 59th Ann. Internat. Mtg., Soc. Expl. Geophys., Expanded Abstracts, 713–715.
Sheriff, R. E., 1975, Factors affecting seismic amplitudes: Geophys. Prosp., **23**, 159–186.
Sherwood, J., 1983, Synthetic seismograms with offset for a layered elastic medium: Offshore Technology Conference, Paper Offshore Tech. Conf., 4508.
Sherwood, J., Hilterman, F. J., Neale, R., and Chen, K. C., 1983, Synthetic seismograms with offset for a layered elastic medium: 53rd Ann. Internat. Mtg., Soc. Expl. Geophys., Expanded Abstracts, 444–447.
Silva, R., and Ahmed, H., 1989, Application of AVO technique in production geophysics., 59th Ann. Internat. Mtg., Soc. Expl. Geophys., Expanded Abstracts, 836–838.
Singh, S. C., West, G. F., and Bregman, N. D., 1989, Full waveform inversion of reflection data: J. Geophys. Res., **94**, 1777–1794.
Snyder, A. G., and Wrolstad, K. H., 1992, Direct detection using AVO, Central Graben, North Sea: Geophysics, **57**, 313–323.
Swan, H. W., 1990, Noise sensitivity of linear seismic inversion: 60th Ann. Internat. Mtg., Soc. Expl. Geophys., Expanded Abstracts, 1177–1180.
Tarantola, A., 1986, A strategy for nonlinear elastic inversion of seismic reflection data: 56th Ann. Internat. Mtg., Soc. Expl. Geophys., Expanded Abstracts, 527–530.
Tatham, R. H., and Stoffa, P. L., 1976, V_p/V_s—A potential hydrocarbon indicator: Geophysics, **41**, 837–849.
Thomsen, L., and Tatham, R., 1983, The change in reflection coefficient with angle of incidence: 53rd Ann. Internat. Mtg., Soc. Expl. Geophys., Expanded Abstracts, 636.
Tooley, R. D., Spencer, T. W., and Sagoci, H. F., 1965, Reflection and transmission of plane compressional waves: Geophysics, **30**, 552–570.
Tura, M. A. C., 1990, Multiparameter elastic inversion: A stable method: 60th Ann. Internat. Mtg., Soc. Expl. Geophys., Expanded Abstracts, 1170–1172.
Ursin, B., 1989, Offset-dependent geometrical spreading in a layered medium: 59th Ann. Internat. Mtg., Soc. Expl. Geophys., Expanded Abstracts, 1156–1159.
Ursin, B., 1990, Least-squares estimation of reflectivity polynomials: 60th Ann. Internat. Mtg., Soc. Expl. Geophys., Expanded Abstracts, 1069–1071.
Vail, P. J., Strauss, P. J., Levitt, P. R., Smith, G. C., and Gidlow, P. M., 1990, Extraction of *P*- and *S*-wave velocities from a 3-D reflection data set and its application to direct hydrocarbon detection: 60th Ann. Internat. Mtg., Soc. Expl. Geophys., Expanded Abstracts, 1181–1184.
Wright, J., 1987, The effects of transverse isotropy on reflection amplitude versus offset: Geophysics, **52**, 564–567.
Young, C. Y., Jarrard, R. D., and Kan, T. K., 1983, Prestack synthetic seismogram of elastic-layered earth: 53rd Ann. Internat. Mtg., Soc. Expl. Geophys., Expanded Abstracts, 455–457.
Yu, G., 1985(b), Offset-amplitude variation and controlled amplitude processing: Geophysics, **50**, 2697–2708.

APPENDIX A—MATRIX REPRESENTATION OF THE KNOTT-ZOEPPRITZ EQUATIONS

Aki and Richards (1980) give the Knott-Zoeppritz equations in convenient matrix form. For completeness they are repeated here.

For an interface between two infinite elastic half-spaces, there are sixteen reflection and transmission coefficients (see Figure A-1). In the Aki and Richards notation, the coefficients are represented by two letters (e.g. $\grave{P}\acute{S}$). The first letter indicates the type of incident wave and the second letter represents the type of derived wave. The acute accent ($\acute{}$) indicates an upgoing wave while a downgoing wave has a grave accent ($\grave{}$). Thus, $\grave{P}\acute{S}$ is the downgoing *P*-wave to upgoing *S*-wave coefficient. With this notation, the scattering matrix is

$$\mathbf{Q} = \begin{pmatrix} \grave{P}\acute{P} & \grave{S}\acute{P} & \acute{P}\acute{P} & \acute{S}\acute{P} \\ \grave{P}\acute{S} & \grave{S}\acute{S} & \acute{P}\acute{S} & \acute{S}\acute{S} \\ \grave{P}\grave{P} & \grave{S}\grave{P} & \acute{P}\grave{P} & \acute{S}\grave{P} \\ \grave{P}\grave{S} & \grave{S}\grave{S} & \acute{P}\grave{S} & \acute{S}\grave{S} \end{pmatrix} = \underset{\sim}{\mathbf{P}}^{-1}\underset{\sim}{\mathbf{R}} \qquad \text{(A-1)}$$

where $\underset{\sim}{\mathbf{P}}$ is the matrix

$$\begin{pmatrix} -\sin\Theta_1 & -\cos\Phi_1 & \sin\Theta_2 & \cos\Phi_2 \\ \cos\Theta_1 & -\sin\Phi_1 & \cos\Theta_2 & -\sin\Phi_2 \\ 2\rho_1 V_{S1}\sin\Phi_1\cos\Theta_1 & \rho_1 V_{S1}(1-2\sin^2\Phi_1) & 2\rho_2 V_{S2}\sin\Phi_2\cos\Theta_2 & \rho_2 V_{S2}(1-2\sin^2\Phi_2) \\ -\rho_1 V_{P1}(1-2\sin^2\Phi_1) & \rho_1 V_{S1}\sin 2\Phi_1 & \rho_2 V_{P2}(1-2\sin^2\Phi_2) & -\rho_2 V_{S2}\sin 2\Phi_2 \end{pmatrix}$$

and $\underset{\sim}{\mathbf{R}}$ is the matrix

$$\begin{pmatrix} \sin\Theta_1 & \cos\Phi_1 & -\sin\Theta_2 & -\cos\Phi_2 \\ \cos\Theta_1 & -\sin\Phi_1 & \cos\Theta_2 & -\sin\Phi_2 \\ 2\rho_1 V_{S1}\sin\Phi_1\cos\Theta_1 & \rho_1 V_{S1}(1-2\sin^2\Phi_1) & 2\rho_2 V_{S2}\sin\Phi_2\cos\Theta_2 & \rho_2 V_{S2}(1-2\sin^2\Phi_2) \\ \rho_1 V_{P1}(1-2\sin^2\Phi_1) & -\rho_1 V_{S1}\sin 2\Phi_1 & -\rho_2 V_{P2}(1-2\sin^2\Phi_2) & \rho_2 V_{S2}\sin 2\Phi_2 \end{pmatrix}.$$

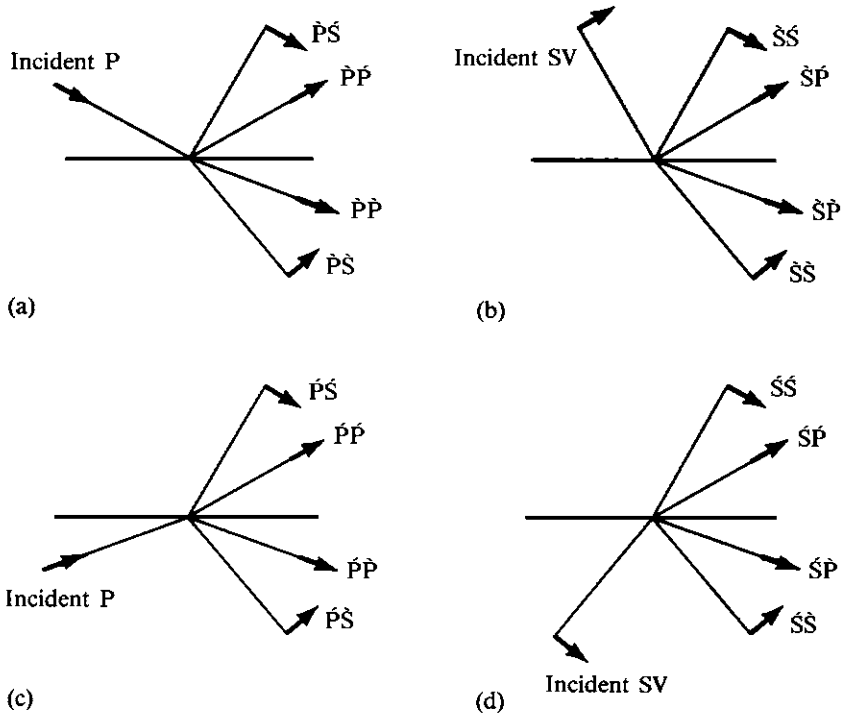

Fig. A-1. Notation for the sixteen possible reflection/transmission coefficients for *P-SV* waves at an interface between two different solid half-spaces. Short arrows show the directions of particle motion (from Aki and Richards, 1980).